Electronic Supplementary Material (ESI) for Dalton Transactions.

Supporting Information

Systematic Size Mediated Trapping of Anions of Varied Dimensionality within Dimeric Capsular Assembly of a Flexible Neutral Bis-Urea Platform

Utsab Manna, Santanu Kayal, Biswajit Nayak and Gopal Das*

Department of Chemistry, Indian Institute of Technology Guwahati,

Assam, 781 039, India.

Fax: +91-361-258-2349; Tel: +91-361-258-2313

Email: gdas@iitg.ernet.in

Table of Contents

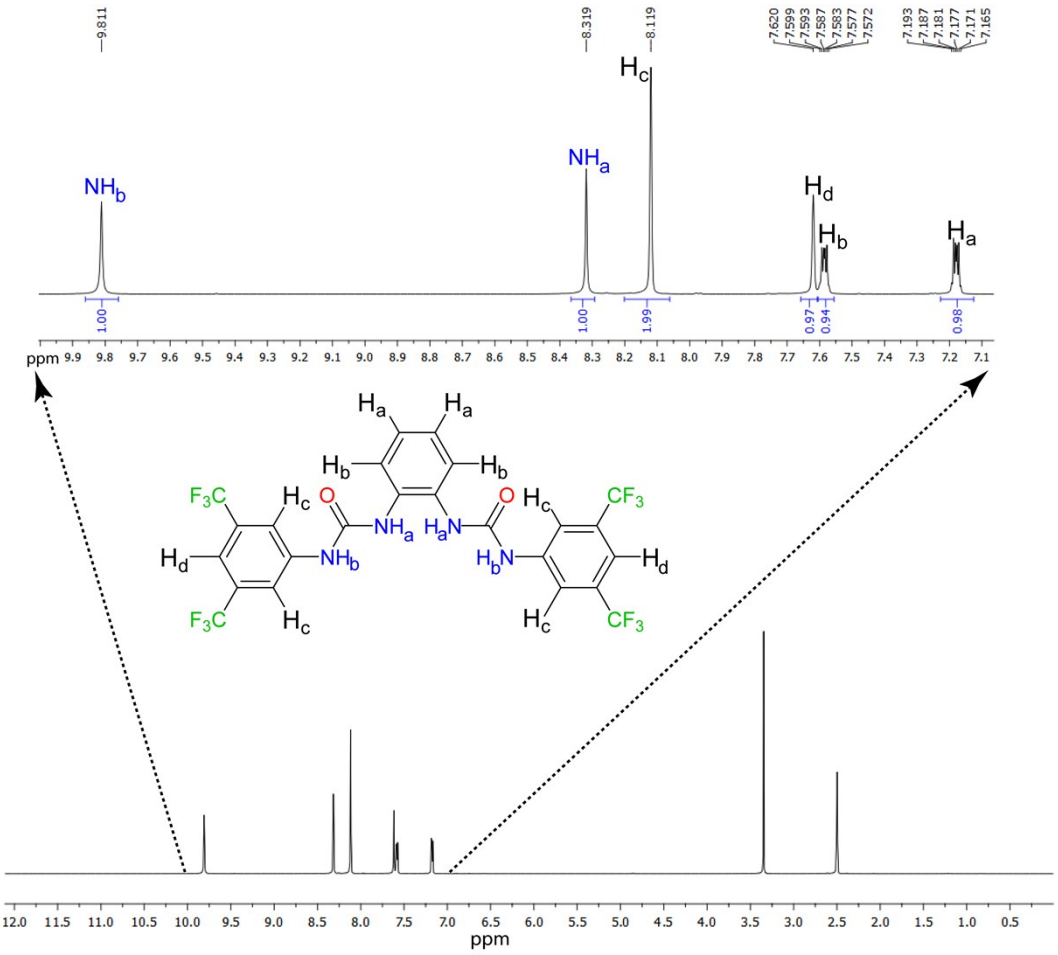

Figure S1. ^{1}H NMR spectrum of receptor **L** at 25ºC and interpretation of all hydrogen atoms of the receptor (600 MHz, DMSO-d_6) δ (ppm): 7.165-7.193 (m, 2H, Ar-H), 7.572-7.599 (m, 2H, Ar-H), 7.620 (s, 4H, Ar-H), 8.119 (s, 2H, Ar-H), 8.319 (s, 2H, NH_a), 9.811 (s, 2H, NH_b).

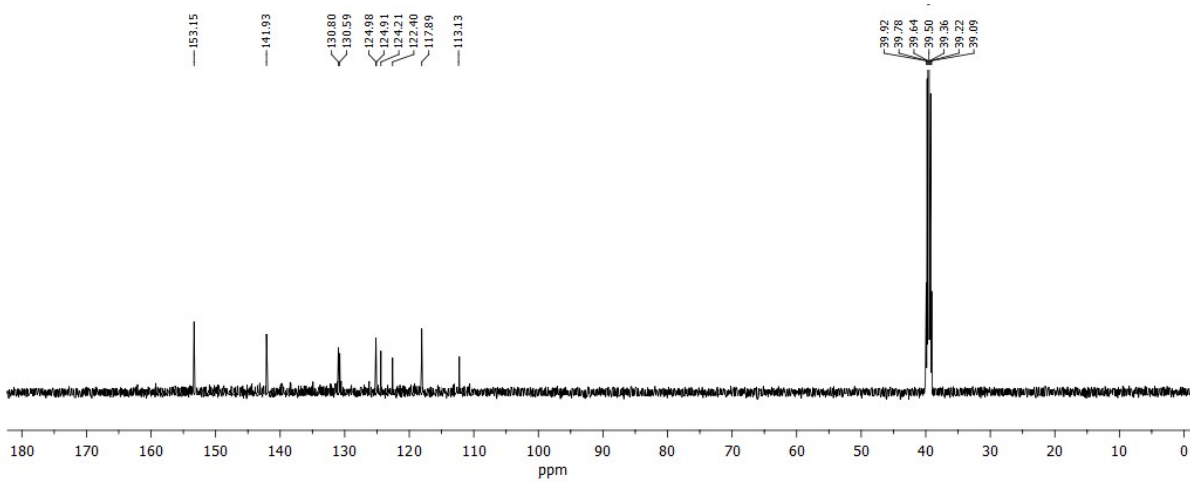

Figure S2. ^{13}C NMR spectrum of receptor **L** at 25ºC (150 MHz, DMSO-d_6) δ (ppm): 113.13 (×1C, Ar-C), 117.89 (×1C, Ar-C), 122.40(×2C, Ar-C), 124.21 (×2C, Ar-C), 124.91 (×4C, Ar-C), 124.98 (×4C, Ar-C), 130.59 (×4C, Ar-C), 130.80 (×2C, Ar-C), 141.93 (×2C, Ar), 153.15 (×2C, -C=O).

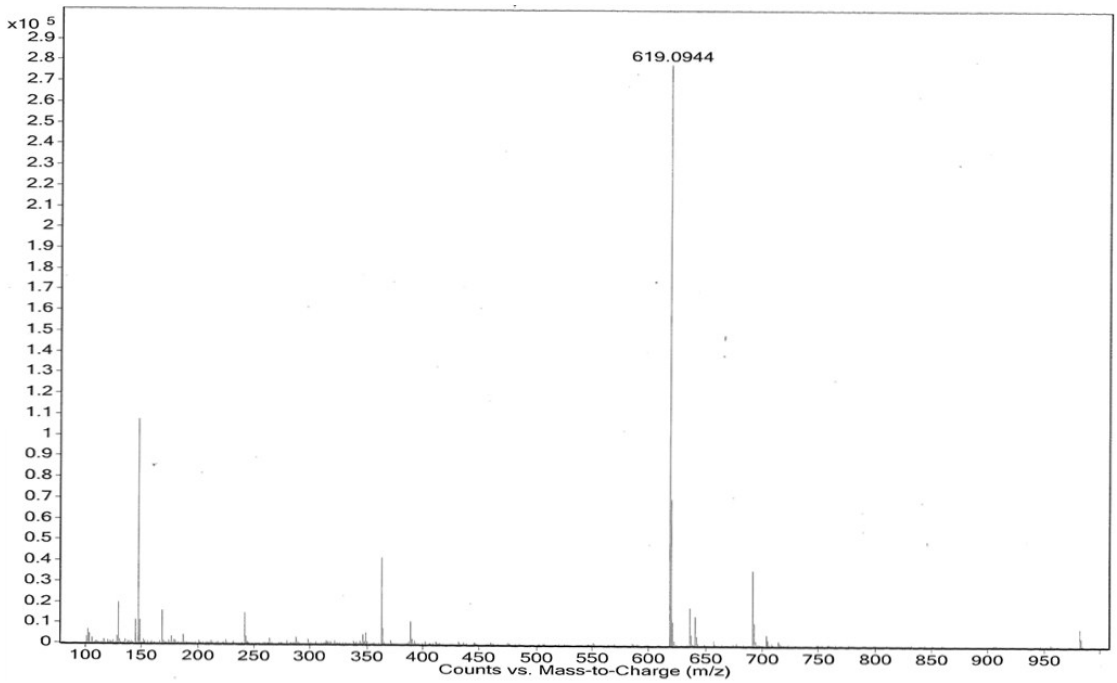

Figure S3. ESI-Mass spectrum of receptor **L.** ESI-MS: m/z 619.0944 [**L**+H].

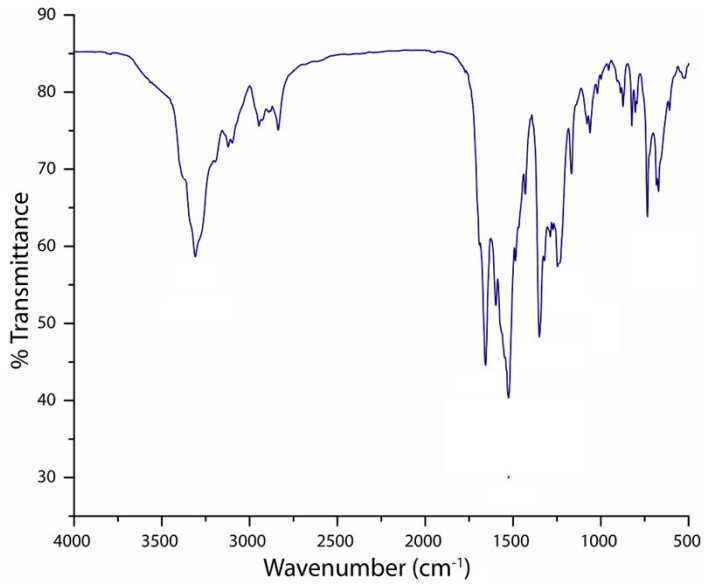

Figure S4. FT-IR spectrum of receptor $\mathbf{L_1}$ recorded in KBr pellet at 25ºC: 3327 cm^{-1} *vs*(N–H), 3138 cm^{-1} *vs*(C-H), 1670 cm^{-1} *vs*(C=O), 1257 cm^{-1} *vs*(C-F).

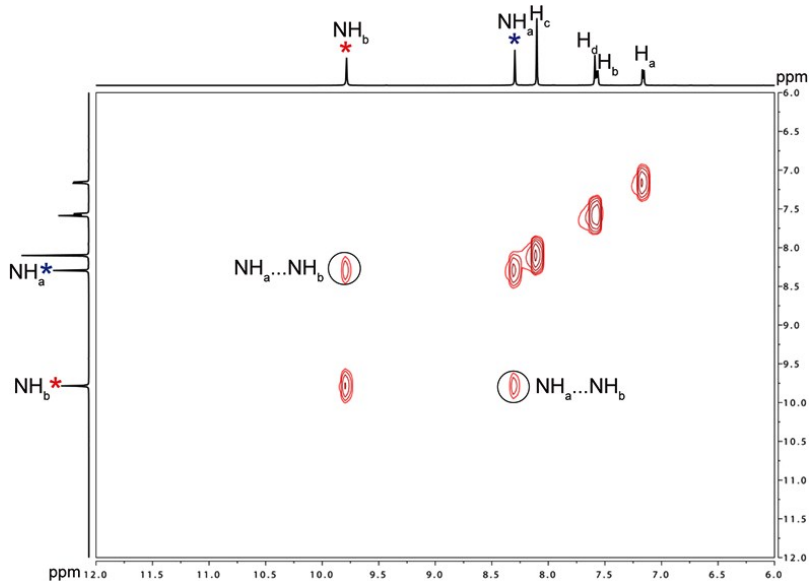

Figure S5. 2D-NOESY NMR spectra of **L** in DMSO-d6 at 298 K

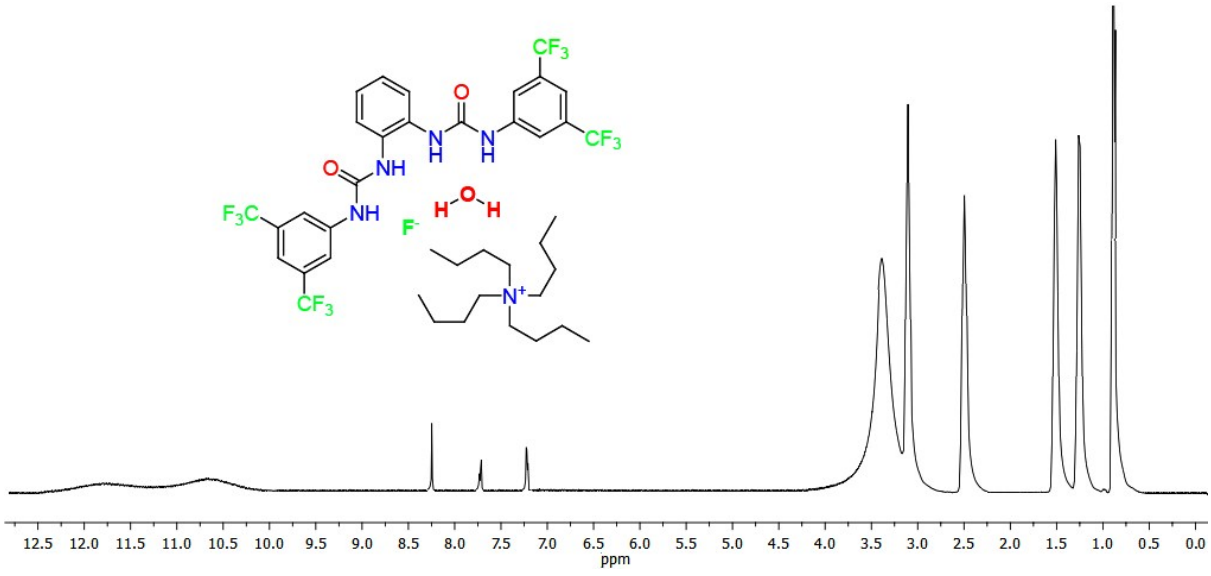

Figure S6. ^{1}H-NMR spectrum of complex **1** in DMSO-d_6 at 25ºC, (600 MHz, DMSO-d_6) δ (ppm): 0.914-0.939 (t, 12H, ~7.8 Hz, TBA-CH_3), 1.269-1.330 (m, 8H, TBA-CH_2), 1.529-1.581 (m, 8H, TBA-CH_2), 3.136-3.165 (t, 8H, ~ 8.4 Hz, N^+-TBA-CH_2), 7.156-7.184 (m, 2H, Ar−H), 7.599-7.627 (m, 2H, Ar−H), 7.596 (s, 4H, Ar-H), 8.114 (s, 2H, Ar-H), 10.685 (s, 2H, NH_a), 11.788 (s, 2H, NH_b).

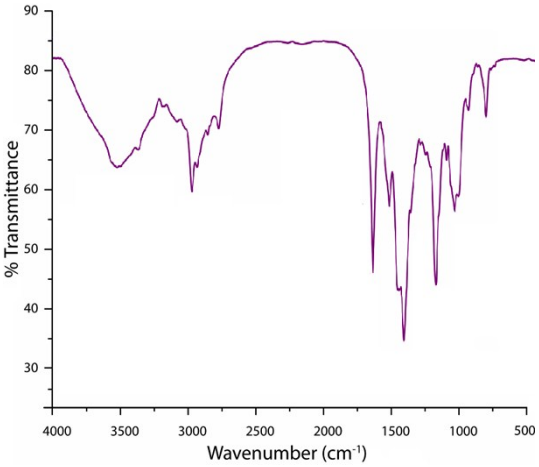

Figure S7. FT-IR spectrum of complex **1** recorded in KBr pellet at 25ºC: 3476 cm^{-1} *vs*(O–H), 3368 cm^{-1} *vs*(N–H) 3028 cm^{-1} *vs* (C-H), 2863 cm^{-1} *vs*(C-H), 1674 cm^{-1} *vs*(C=O), 1268 cm^{-1} *vs*(C-F).

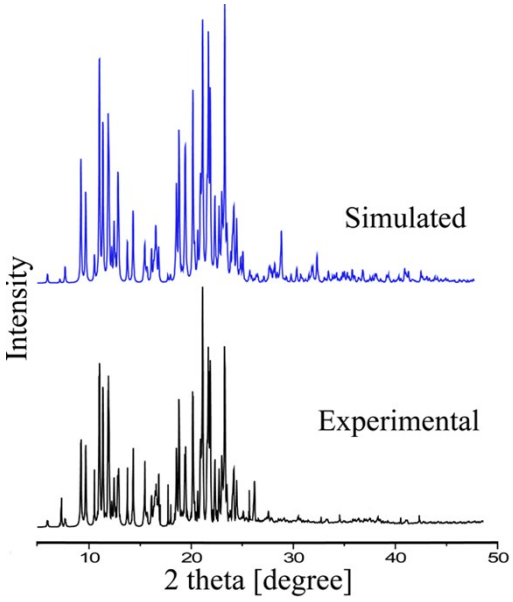

Figure S8. Powder X-ray diffraction: simulated pattern from the single-crystal X-ray of complex **1** (blue), experimental pattern from the crystalline solid of complex **1** (black).

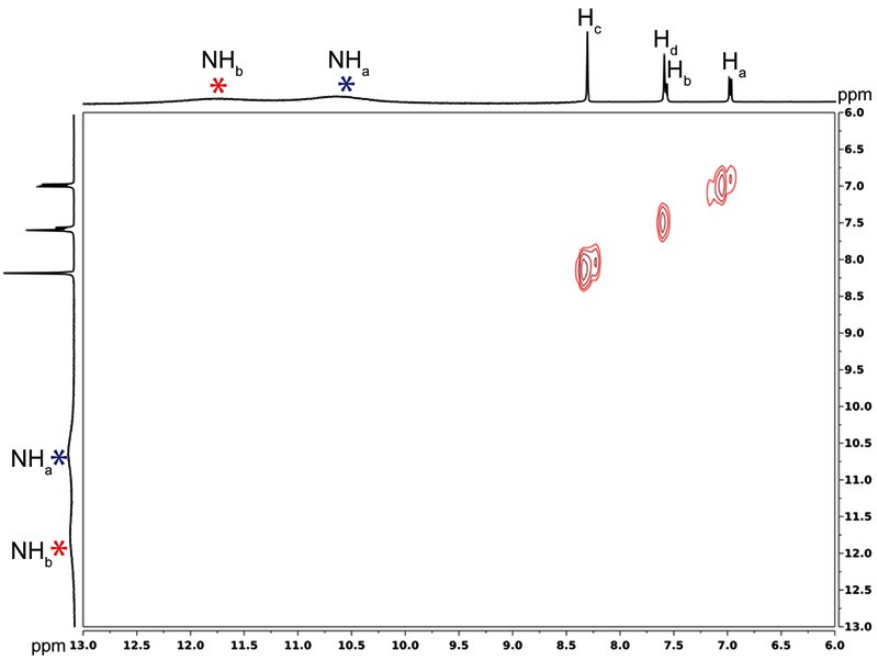

Figure S9. 2D-NOESY NMR spectra of complex **1** in DMSO-d_6 at 298 K.

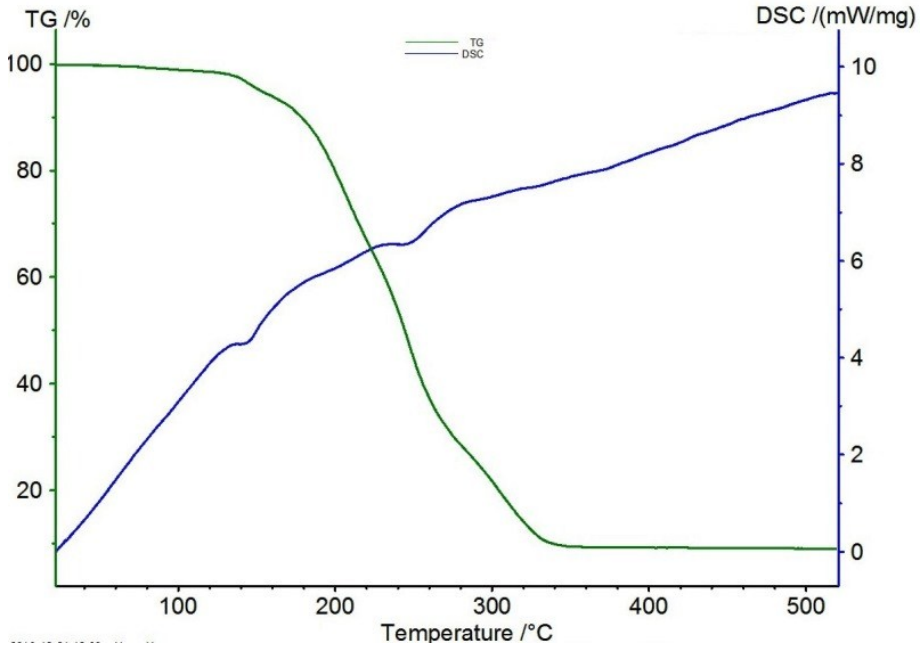

Figure S10. Thermo gravimetric (TGA) and Diffrential scanning calorimetry (DSC) curve of only hydrated-fluoride complex **1** obtained at a heating rate of 10˚C/min in N_2 atmosphere.

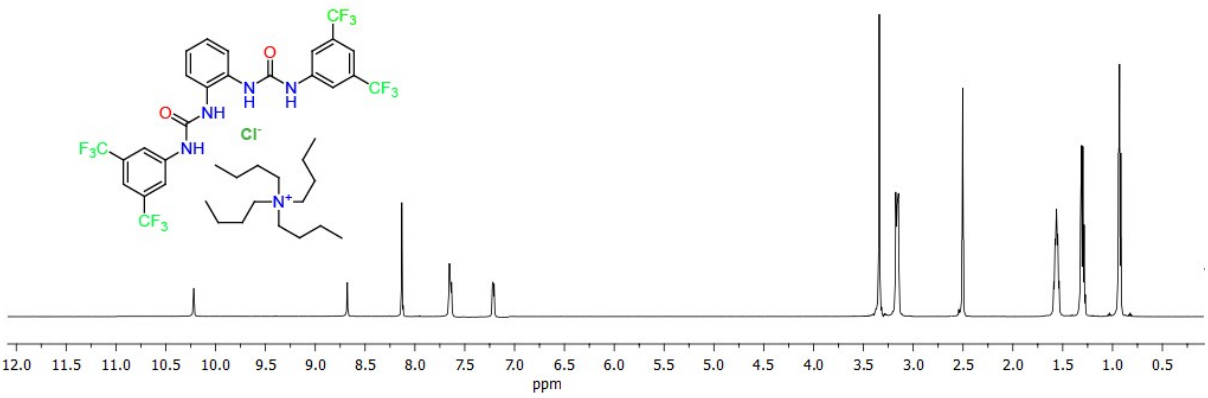

Figure S11. ^{1}H-NMR spectrum of complex **2a** in DMSO-d_6 at 25ºC, (600 MHz, DMSO-d_6) δ (ppm): 0.914-0.938 (t, 12H, ~7.2 Hz, TBA-CH_3), 1.270-1.331 (m, 8H, TBA-CH_2), 1.533-1.586 (m, 8H, TBA-CH_2), 3.144-3.172 (t, 8H, ~ 8.4 Hz, N^+-TBA-CH_2), 7.154-7.183 (m, 2H, Ar-H), 7.596-7.625 (m, 2H, Ar-H), 7.623 (s, 4H, Ar-H), 8.128 (s, 2H, Ar-H), 8.636 (s, 2H, NH_a), 10.246 (s, 2H, NH_b).

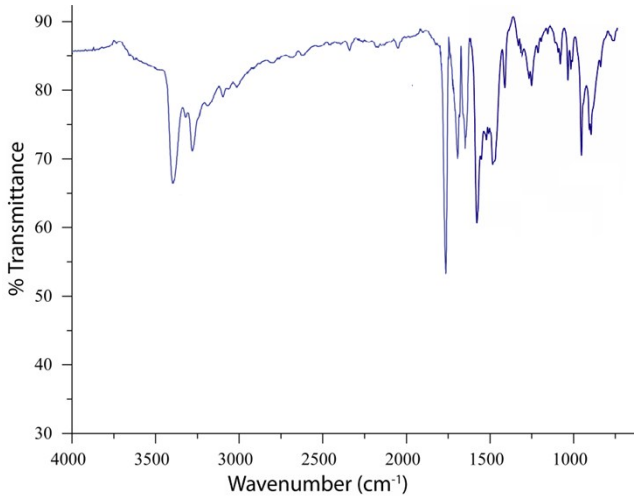

Figure S12. FT-IR spectrum of complex **2a** recorded in KBr pellet at 25ºC: 3354 cm^{-1} *vs*(N–H) 3024 cm^{-1} *vs* (C-H), 2850 cm^{-1} *vs*(C-H), 1668 cm^{-1} *vs*(C=O), 1256 cm^{-1} *vs*(C-F).

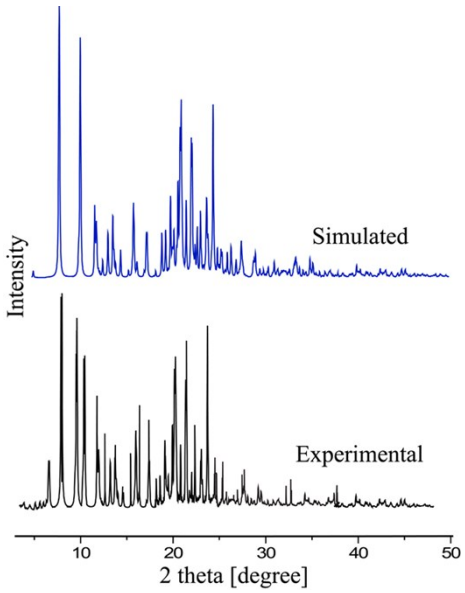

Figure S13. Powder X-ray diffraction: simulated pattern from the single-crystal X-ray of complex **2a** (blue), experimental pattern from the crystalline solid of complex **2a** (black).

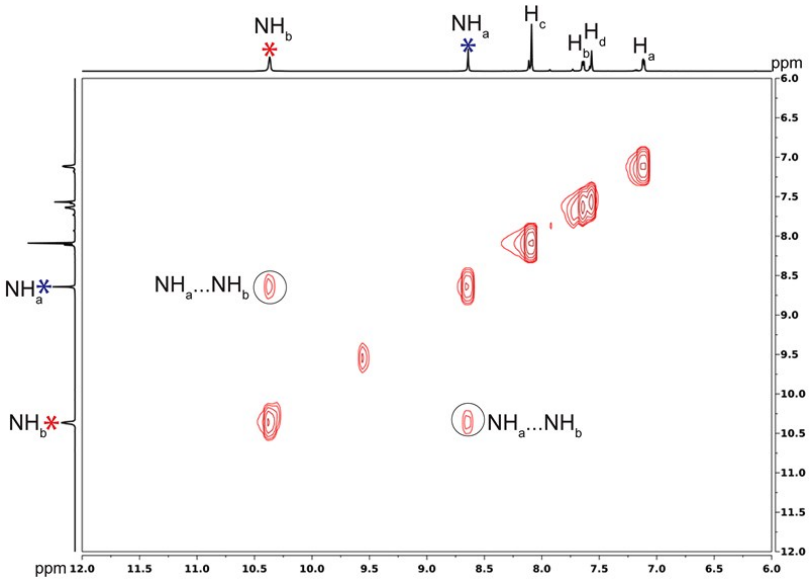

Figure S14. 2D-NOESY NMR spectra of complex **2a** in DMSO-d_6 at 298 K.

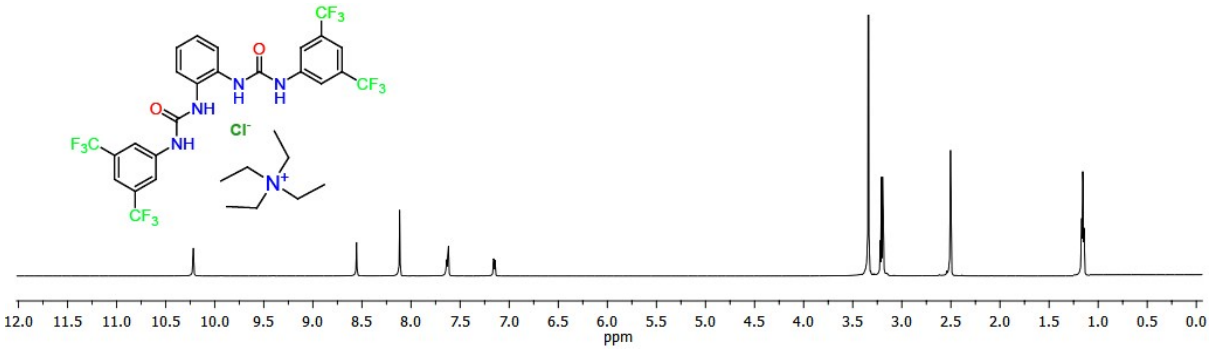

Figure S15. ^{1}H-NMR spectrum of complex **2b** in DMSO-d_6 at 25ºC, (600 MHz, DMSO-d_6) δ (ppm): 1.141-1.165 (t, 12H, ~7.2 Hz, TEA-CH_3), 3.181-3.217 (q, 8H, ~7.2 Hz, N^+-TEA-CH_2), 7.135-7.162 (m, 2H, Ar−H), 7.614-7.644 (m, 2H, Ar−H), 7.615 (s, 4H, Ar-H), 8.112 (s, 2H, Ar-H), 8.355 (s, 2H, NH_a), 10.218 (s, 2H, NH_b).

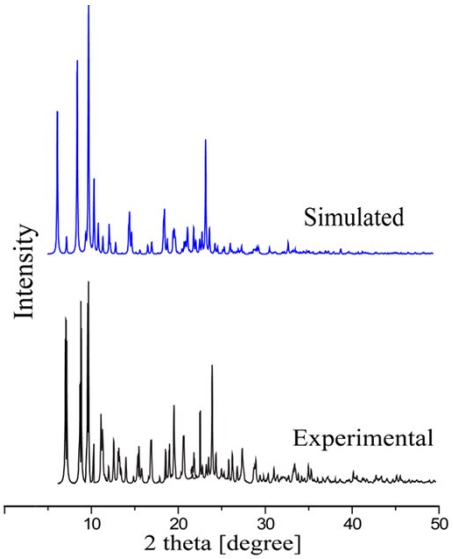

Figure S16. Powder X-ray diffraction: simulated pattern from the single-crystal X-ray of complex **2b** (blue), experimental pattern from the crystalline solid of complex **2b** (black).

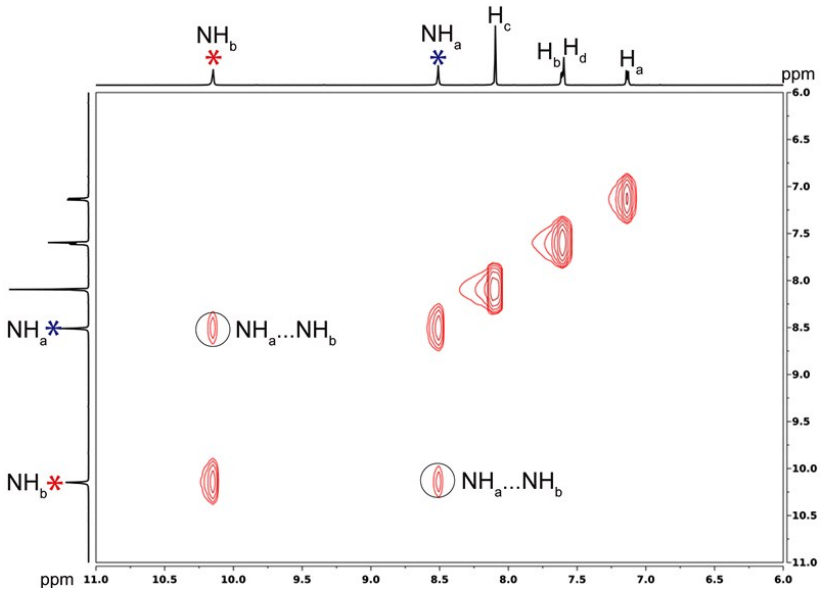

Figure S17. 2D-NOESY NMR spectra of complex **2b** in DMSO-d_6 at 298 K.

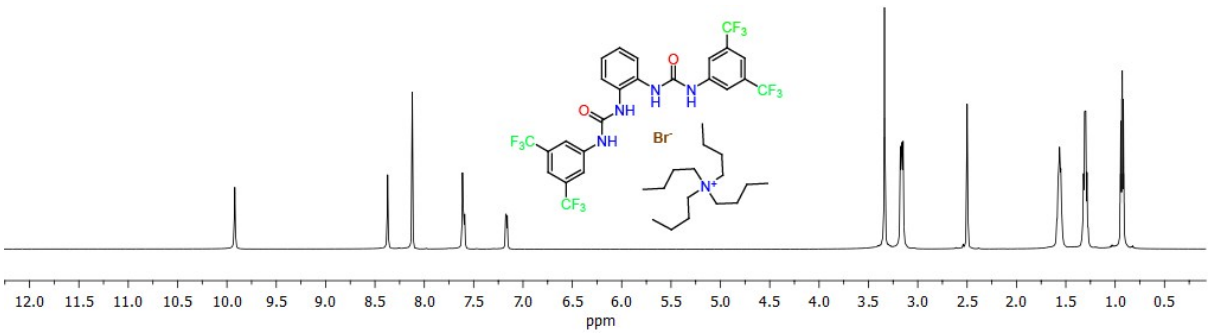

Figure S18. ^{1}H-NMR spectrum of complex **3** in DMSO-d_6 at 25ºC, (600 MHz, DMSO-d_6) δ (ppm): 0.917-0.942 (t, 12H, ~7.8 Hz, TBA-CH_3), 1.273-1.334 (m, 8H, TBA-CH_2), 1.538-1.589 (m, 8H, TBA-CH_2), 3.148-3.176 (t, 8H, ~ 8.4 Hz, N^+-TBA-CH_2), 7.154-7.182 (m, 2H, Ar-H), 7.585-7.613 (m, 2H, Ar−H), 7.613 (s, 4H, Ar-H), 8.121 (s, 2H, Ar-H), 8.121 (s, 2H, NH_a), 9.920 (s, 2H, NH_b).

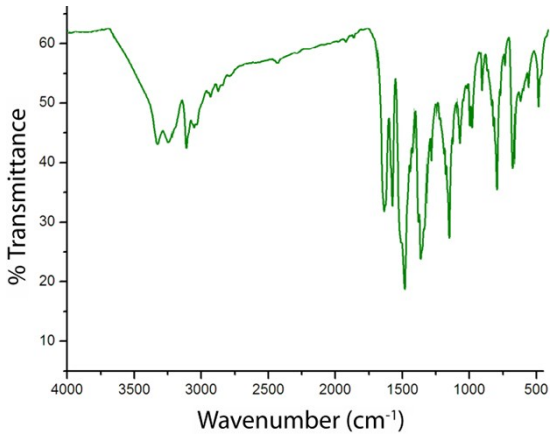

Figure S19. FT-IR spectrum of complex **3** recorded in KBr pellet at 25ºC: 3350 cm^{-1} *vs*(N–H) 3031 cm^{-1} *vs* (C-H), 2853 cm^{-1} *vs*(C-H), 1670 cm^{-1} *vs*(C=O), 1244 cm^{-1} *vs*(C-F).

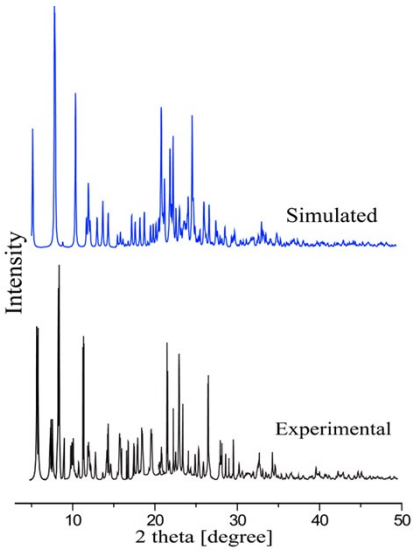

Figure S20. Powder X-ray diffraction: simulated pattern from the single-crystal X-ray of complex **3** (blue), experimental pattern from the crystalline solid of complex **3** (black).

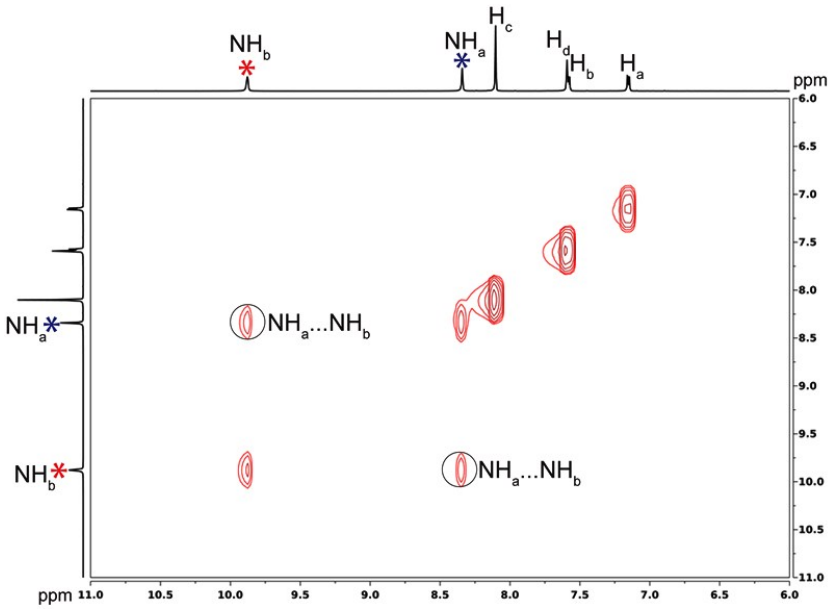

Figure S21. 2D-NOESY NMR spectra of complex **3** in DMSO-d_6 at 298 K.

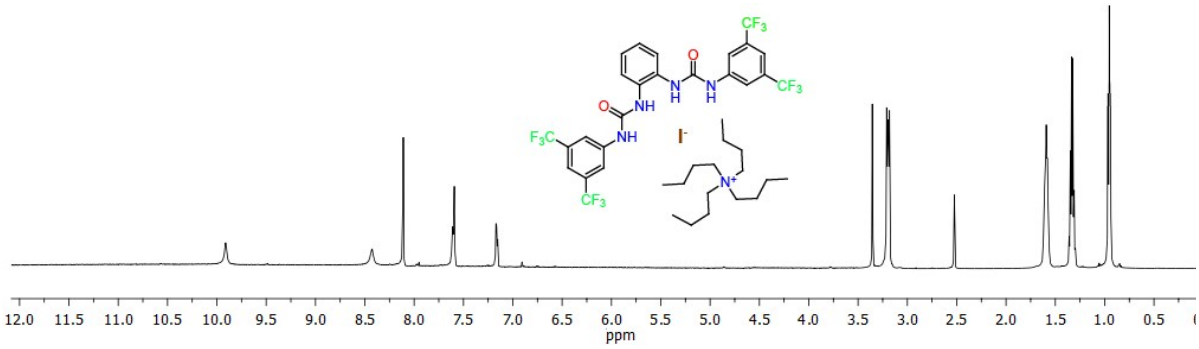

Figure S22. ^{1}H-NMR spectrum of complex **4** in DMSO-d_6 at 25ºC, (400 MHz, DMSO-d_6) δ (ppm): 0.918-0.942 (t, 12H, ~7.8 Hz, TBA-CH_3), 1.275-1.336 (m, 8H, TBA-CH_2), 1.542-1.594 (m, 8H, TBA-CH_2), 3.158-3.186 (t, 8H, ~ 8.4 Hz, N^+-TBA-CH_2), 7.149-7.177 (m, 2H, Ar-H), 7.593 (s, 4H, Ar-H), 7.595-7.622 (m, 2H, Ar-H), 8.111 (s, 2H, Ar-H), 8.427 (s, 2H, NH_a), 9.911 (s, 2H, NH_b).

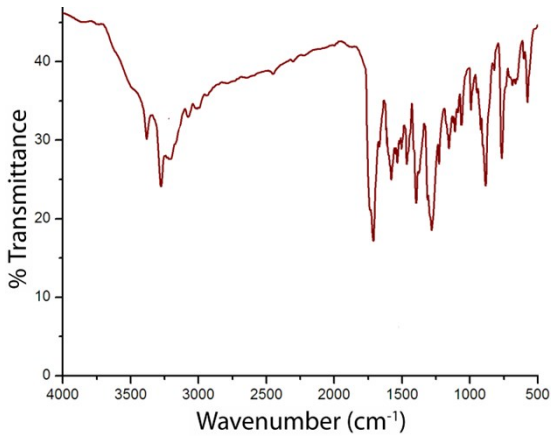

Figure S23. FT-IR spectrum of complex **4** recorded in KBr pellet at 25ºC: 3338 cm^{-1} *vs*(C–H) 3034 cm^{-1} *vs* (C-H), 2858 cm^{-1} *vs*(C-H), 1677 cm^{-1} *vs*(C=O), 1237 cm^{-1} *vs*(C-F).

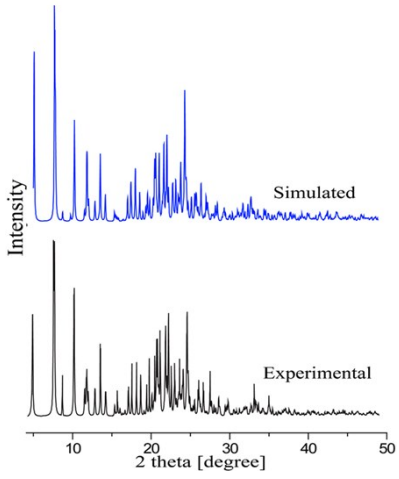

Figure S24. Powder X-ray diffraction: simulated pattern from the single-crystal X-ray of complex **4** (blue), experimental pattern from the crystalline solid of complex **4** (black).

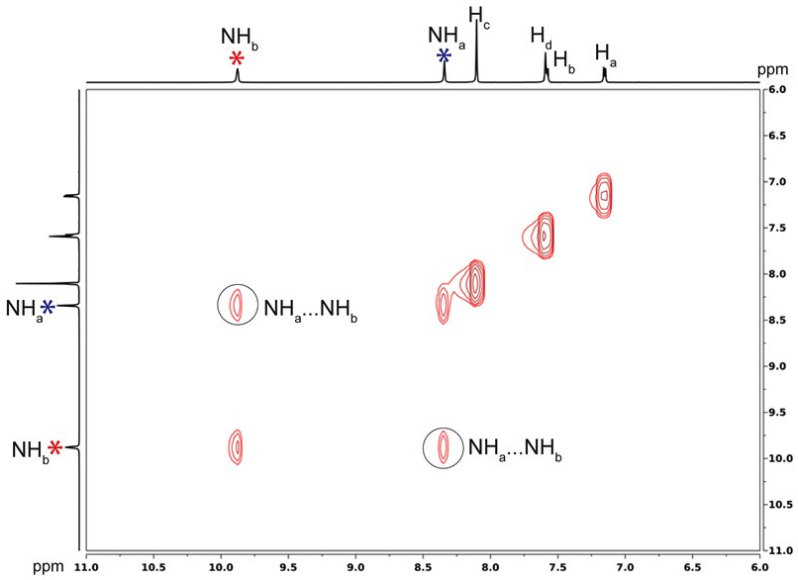

Figure S25. 2D-NOESY NMR spectra of complex **4** in DMSO-d_6 at 298 K.

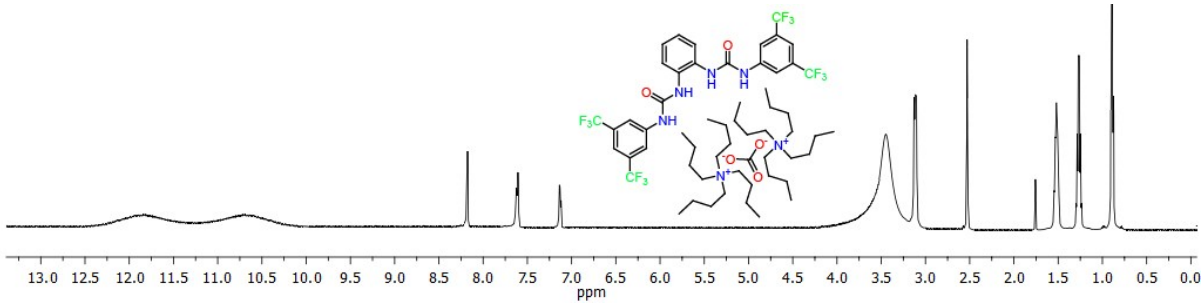

Figure S26. ^{1}H-NMR spectrum of complex **5** in DMSO-d_6 at 25ºC, (600 MHz, DMSO-d_6) δ (ppm): 0.912-0.937 (t, 24H, ~7.2 Hz, TBA-CH_3), 1.267-1.328 (m, 16H, TBA-CH_2), 1.527-1.580 (m, 16H, TBA-CH_2), 3.135-3.163 (t, 16H, ~ 8.4 Hz, N^+-TBA-CH_2), 7.158-7.187 (m, 2H, Ar-H), 7.602-7.629 (m, 2H, Ar-H), 7.599 (s, 4H, Ar-H), 8.121 (s, 2H, Ar-H), 10.558 (s, 2H, NH_a), 11.699 (s, 2H, NH_b).

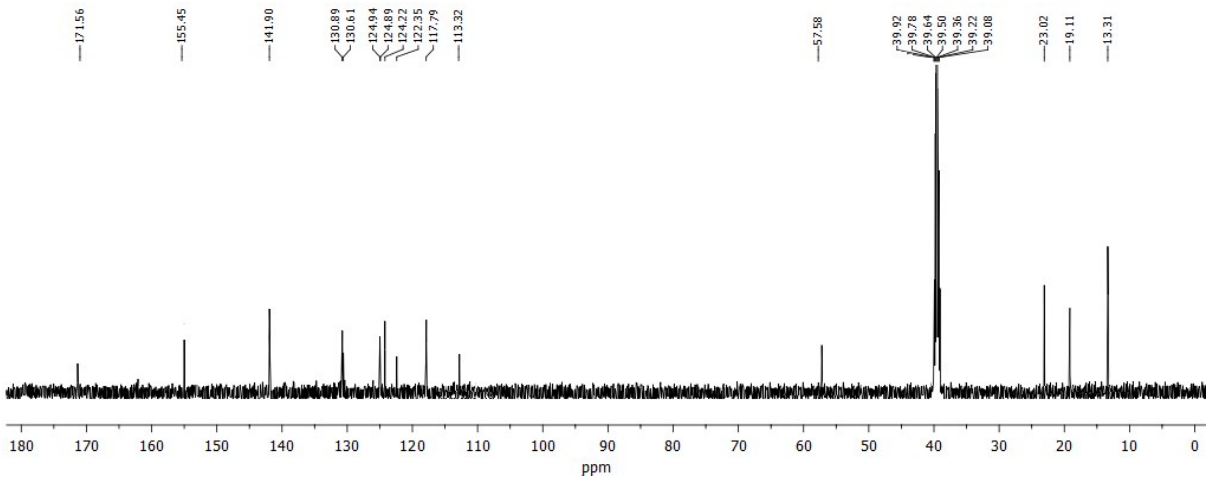

Figure S27. ^{13}C-NMR spectrum of complex **5** in DMSO-d_6 at 25ºC, (150 MHz, DMSO-d_6) δ (ppm): 13.31 (×8C, TBA-CH_3), 19.11 (×8C, TBA-CH_2), 23.02 (×8C, TBA-CH_2), 57.58 (×8C, TBA-N^+CH_2), 113.32 (×1C, Ar-C), 117.79 (×1C, Ar-C), 122.35 (×2C, Ar-C), 124.22 (×2C, Ar-C), 124.89 (×4C, Ar-C), 124.94(×4C, Ar-C), 130.61 (×4C, Ar-C), 130.89 (×2C, Ar-C), 141.90 (×2C, Ar), 155.45 (×2C, -C=O), 171.56 (×1C, Carbonate-C=O).

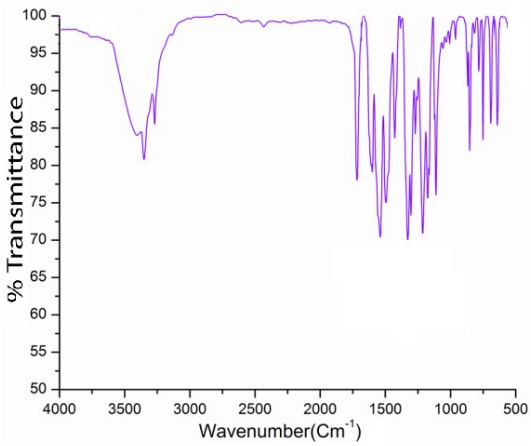

Figure S28. FT-IR spectrum of complex **5** recorded in KBr pellet at 25ºC: IR spectra (KBr pellet): 3382 cm^{-1} *vs*(N–H), 3044 cm^{-1} *vs* (C-H), 2862 cm^{-1} *vs*(C-H), 1665 cm^{-1} *vs*(C=O), 1245 cm^{-1} *vs*(C-F).

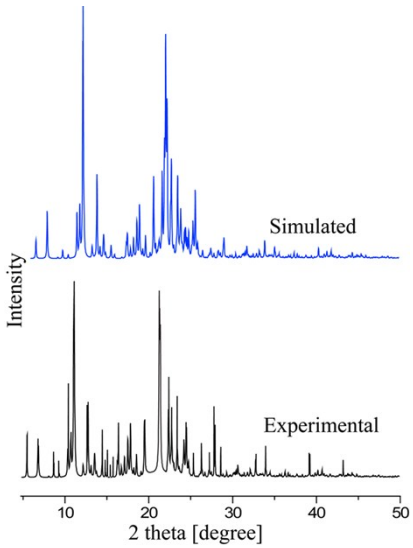

Figure S29. Powder X-ray diffraction: simulated pattern from the single-crystal X-ray of complex **5** (blue), experimental pattern from the crystalline solid of complex **5** (black).

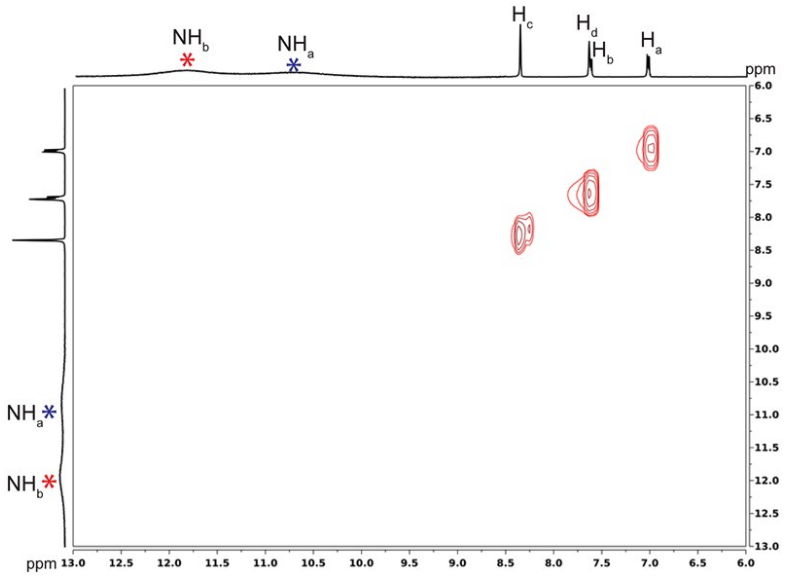

Figure S30. 2D-NOESY NMR spectra of complex **5** in DMSO-d_6 at 298 K.

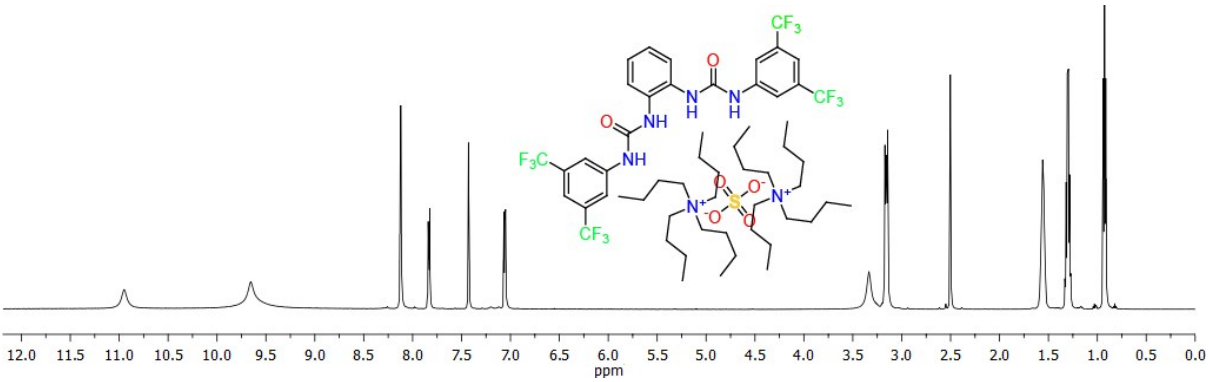

Figure S31. ^{1}H-NMR spectrum of complex **6** in DMSO-d_6 at 25ºC, (600 MHz, DMSO-d_6) δ (ppm): 0.912-0.936 (t, 24H, ~7.2 Hz, TBA-CH_3), 1.267-1.329 (m, 16H, TBA-CH_2), 1.530-1.583 (m, 16H, TBA-CH_2), 3.141-3.169 (t, 16H, ~ 8.4 Hz, N^+-TBA-CH_2), 7.041-7.069 (m, 2H, Ar−H), 7.426 (s, 4H, Ar-H), 7.816-7.844 (m, 2H, Ar−H), 8.119 (s, 2H, Ar-H), 9.651 (s, 2H, NH_a), 10.945 (s, 2H, NH_b).

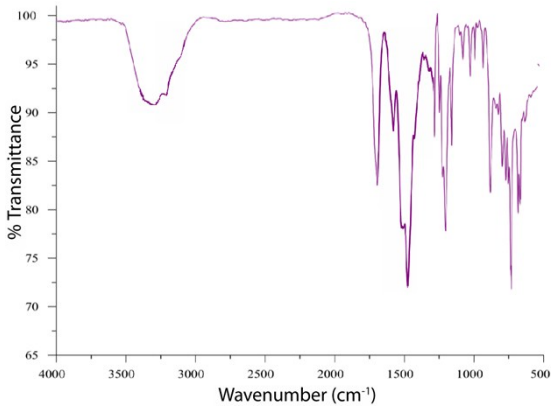

Figure S32. FT-IR spectrum of complex **6** recorded in KBr pellet at 25ºC: 3387 cm^{-1} *vs*(N–H), 3052 cm^{-1} *vs* (C-H), 2857 cm^{-1} *vs*(C-H), 1678 cm^{-1} *vs*(C=O), 1238 cm^{-1} *vs*(C-F).

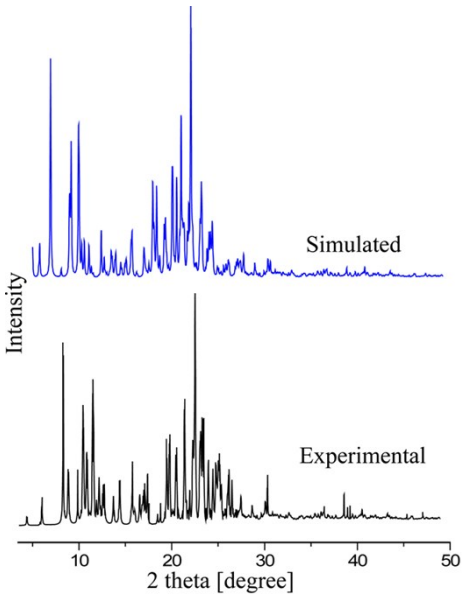

Figure S33. Powder X-ray diffraction: simulated pattern from the single-crystal X-ray of complex **6** (blue), experimental pattern from the crystalline solid of complex **6** (black).

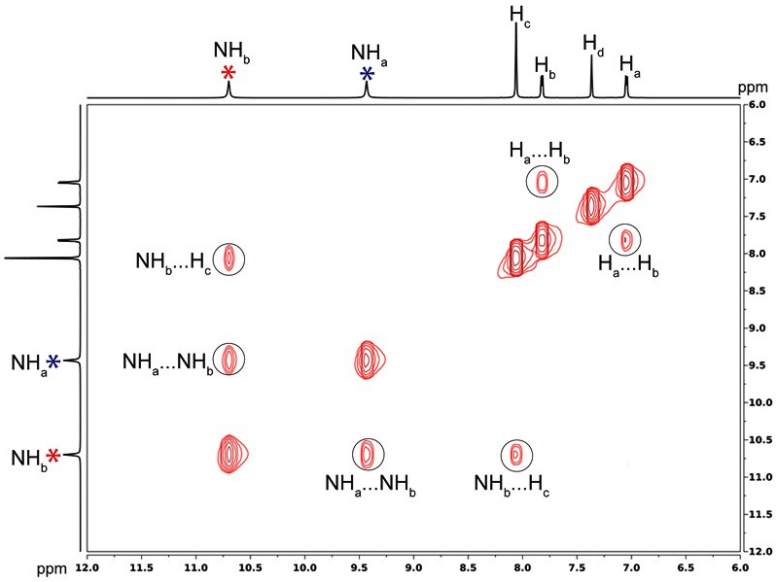

Figure S34. 2D-NOESY NMR spectra of complex **6** in DMSO-d_6 at 298 K.

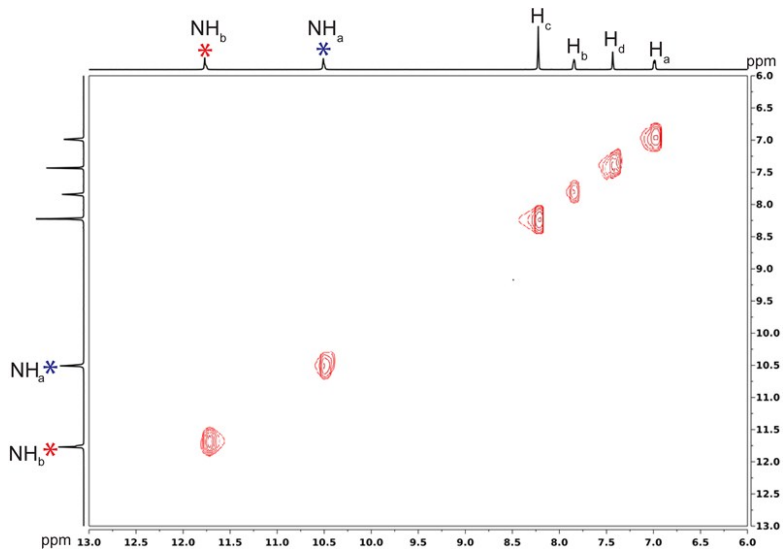

Figure S35. 2D-NOESY NMR spectra of complex **6** in presence of excess *n*-$TBASO_4$ salt in DMSO-d_6 at 298 K.

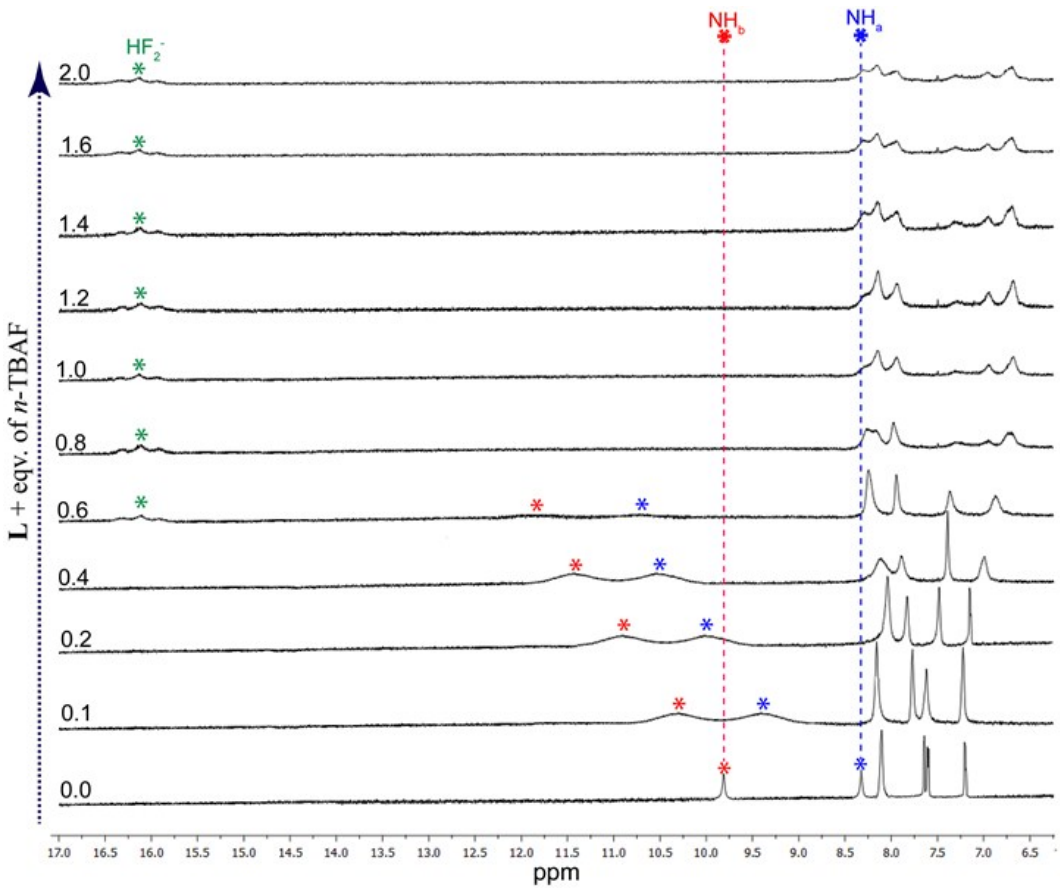

Figure S36. Expanded partial ^{1}H-NMR spectra of **L** upon titration with *n*-TBAF in DMSO-d_6. Disappearance and broadening of urea –NH peaks followed by followed by generation of HF_2^- peak.

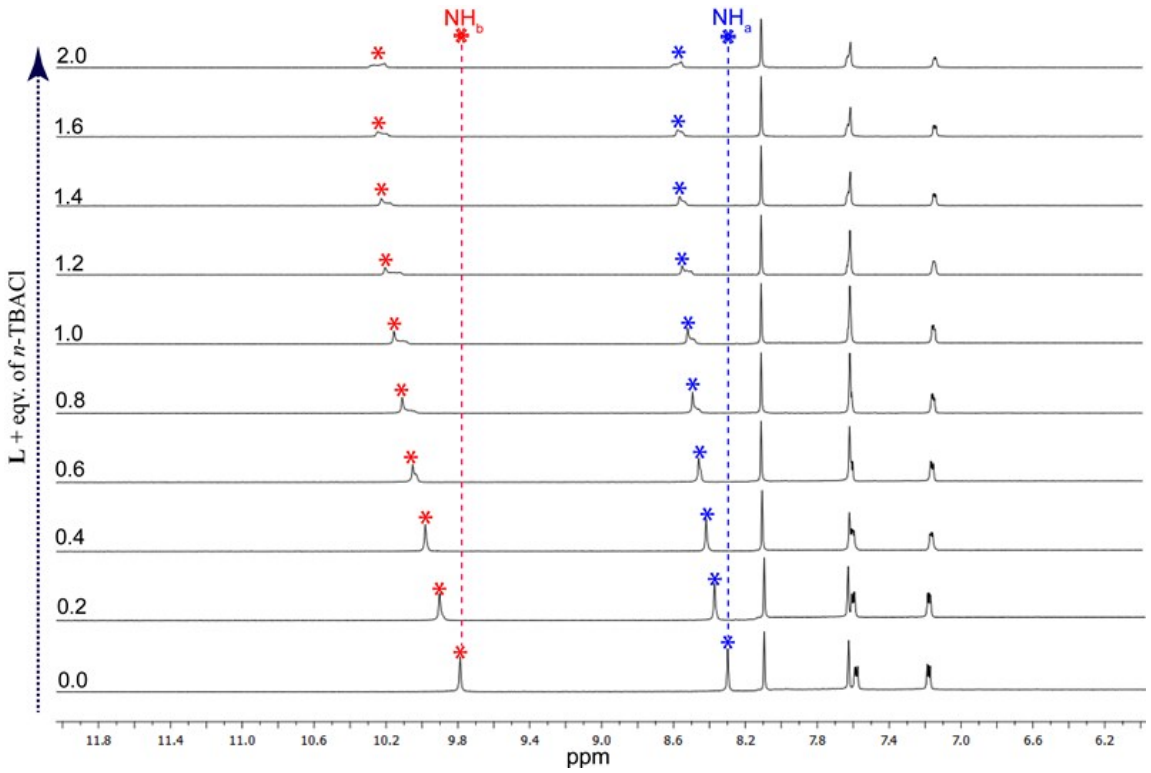

Figure S37. Expanded partial ^{1}H-NMR spectra of **L** upon titration with *n*-TBACl in DMSO-d$_6$.

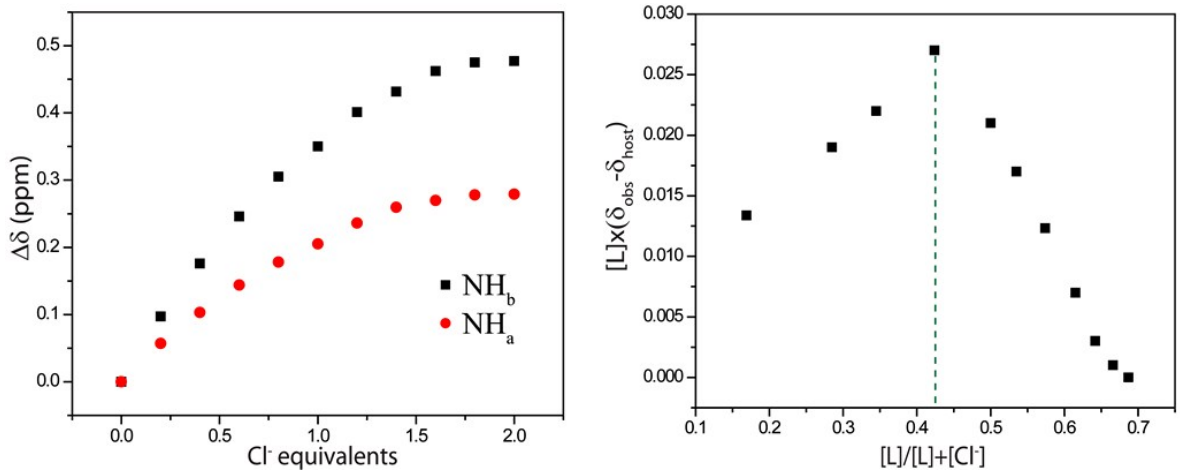

Figure S38. Change in chemical shift of –NH resonances of **L** (10 mM) with increasing conc. of standard Cl$^-$ solution (50 mM) in DMSO-d$_6$ at 298 K and the corresponding Job's plot.

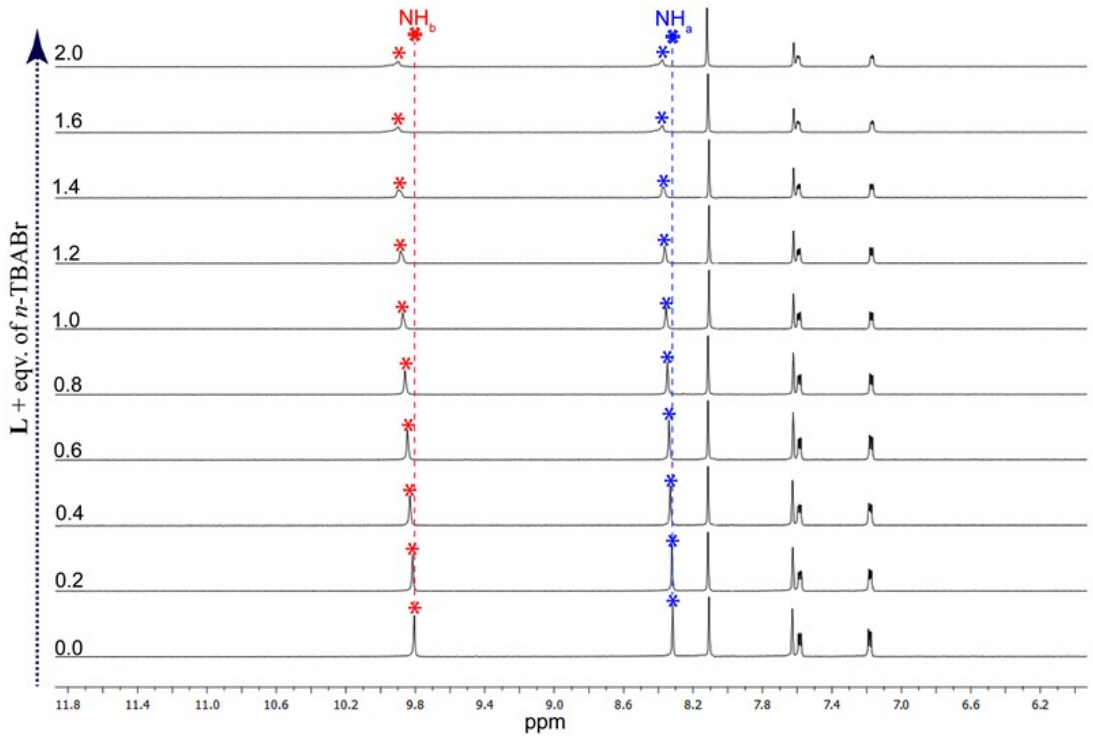

Figure S39. Expanded partial ^{1}H NMR spectra of **L** upon titration with *n*-TBABr in DMSO-d_6 and very negligible shift of urea –NH signals.

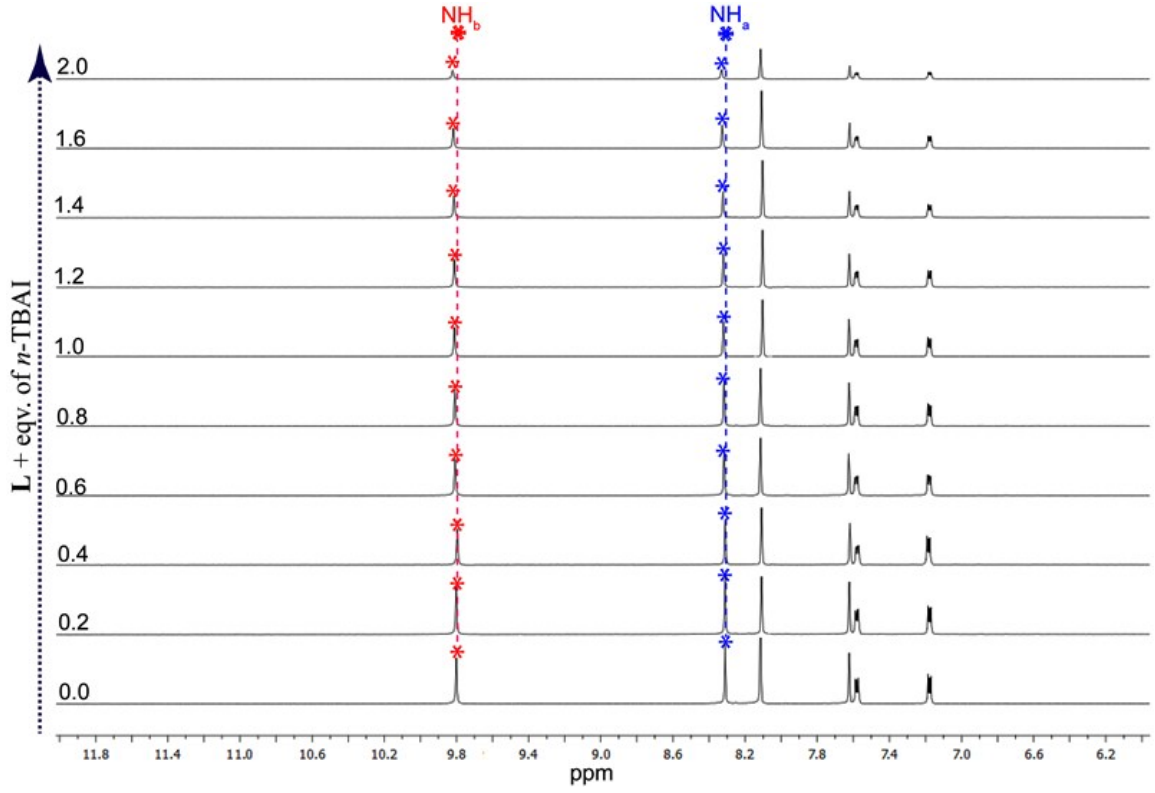

Figure S40. Expanded partial ^{1}H NMR spectra of **L** upon titration with *n*-TBAI in DMSO-d_6 and very negligible shift of urea –NH signals.

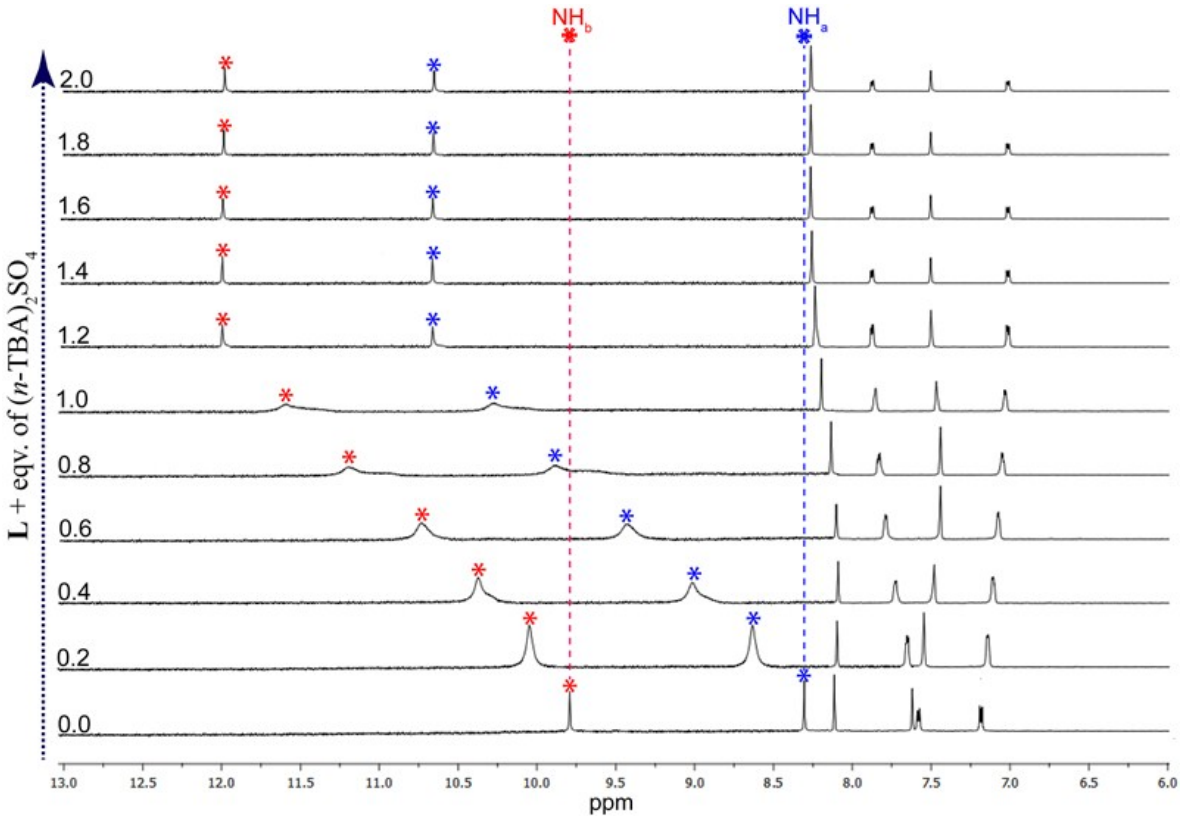

Figure S41. Expanded partial ^{1}H NMR spectra of **L** upon titration with (n-TBA)$_2$SO$_4$ in DMSO-d$_6$.

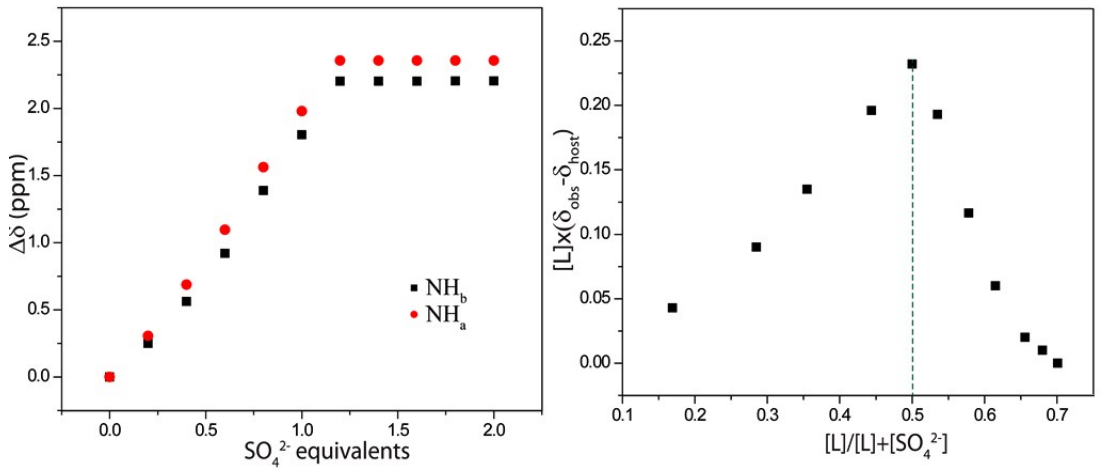

Figure S42. Change in chemical shift of –NH resonances of **L** (10 mM) with increasing conc. of standard SO_4^{2-} solution (50 mM) in DMSO-d$_6$ at 298 K and the corresponding Job's plot.

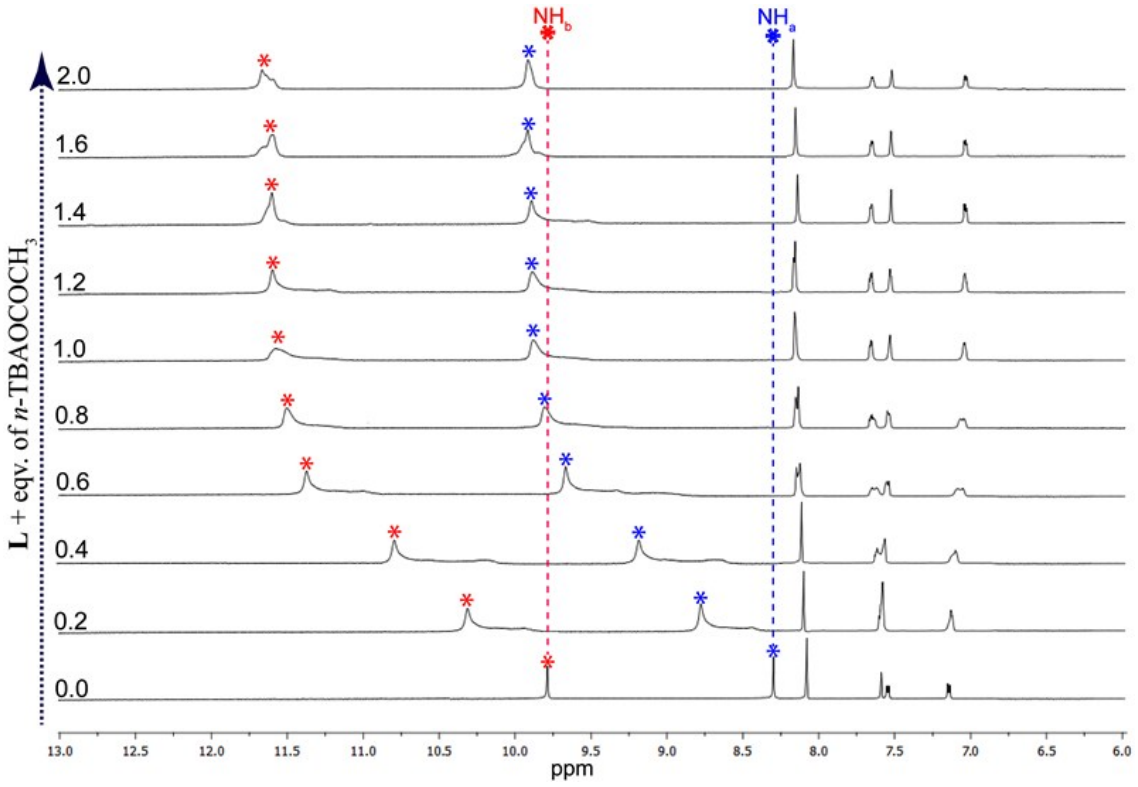

Figure S43. Expanded partial ^{1}H NMR spectra of **L** upon titration with *n*-TBAOCOCH$_3$ in DMSO-d$_6$.

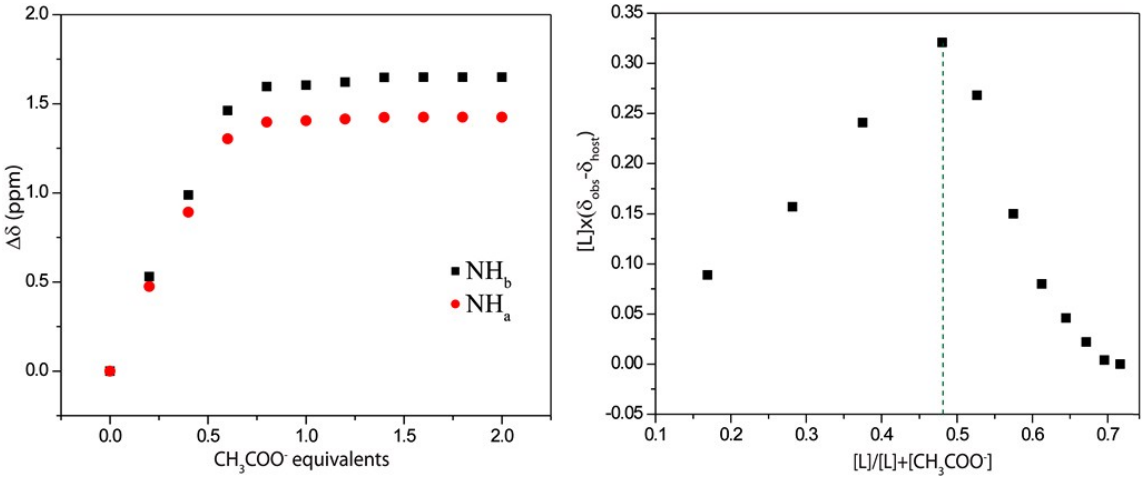

Figure S44. Change in chemical shift of –NH resonances of **L** (10 mM) with increasing conc. of standard CH_3COO^- solution (50 mM) in DMSO-d$_6$ at 298 K and the corresponding Job's plot.

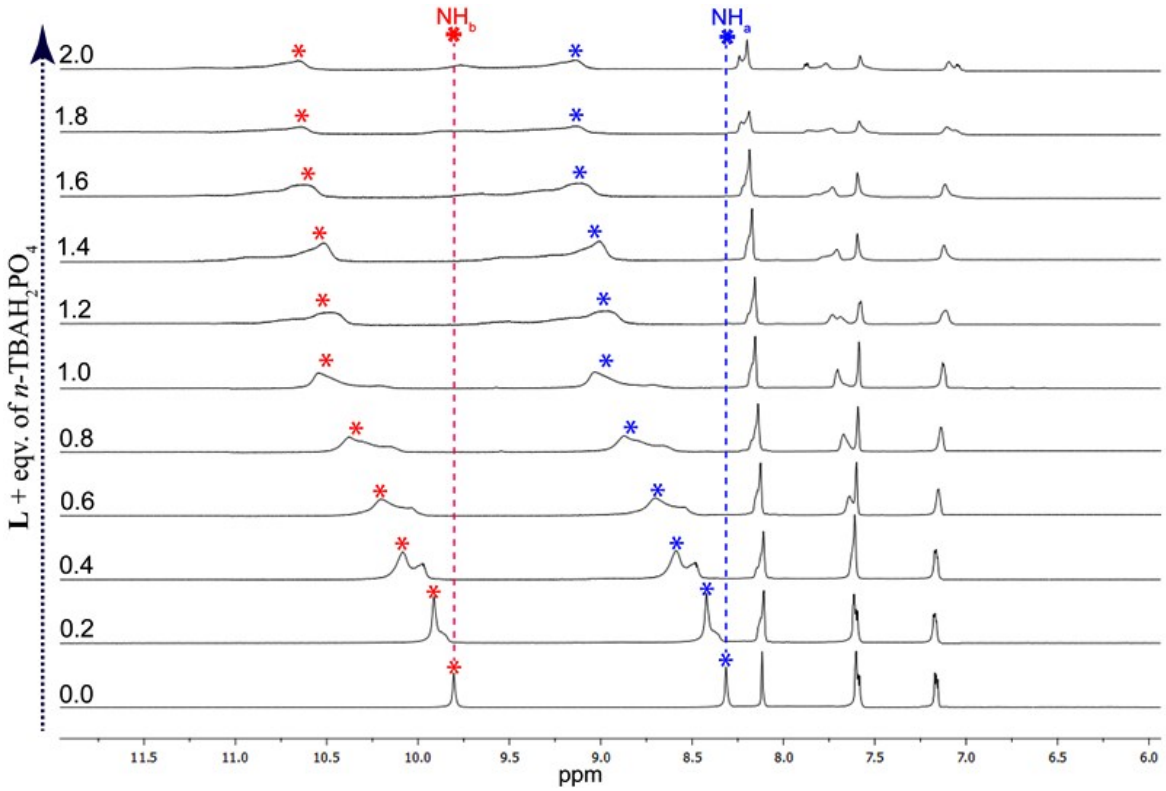

Figure S45. Expanded partial ^{1}H NMR spectra of **L** upon titration with *n*-$TBAH_2PO_4$ in DMSO-d_6.

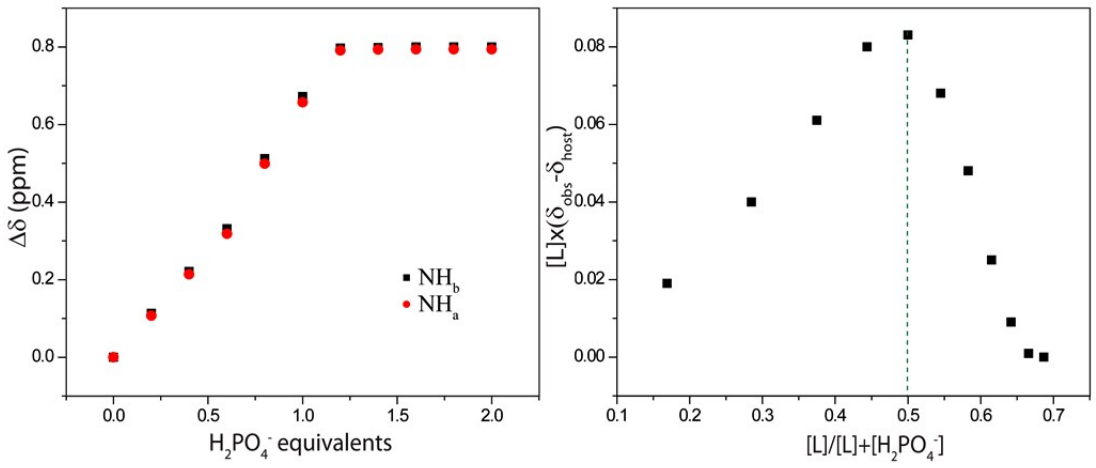

Figure S46. Change in chemical shift of –NH resonances of **L** (10 mM) with increasing conc. of standard $H_2PO_4^-$ solution (50 mM) in DMSO-d_6 at 298 K and the corresponding Job's plot.

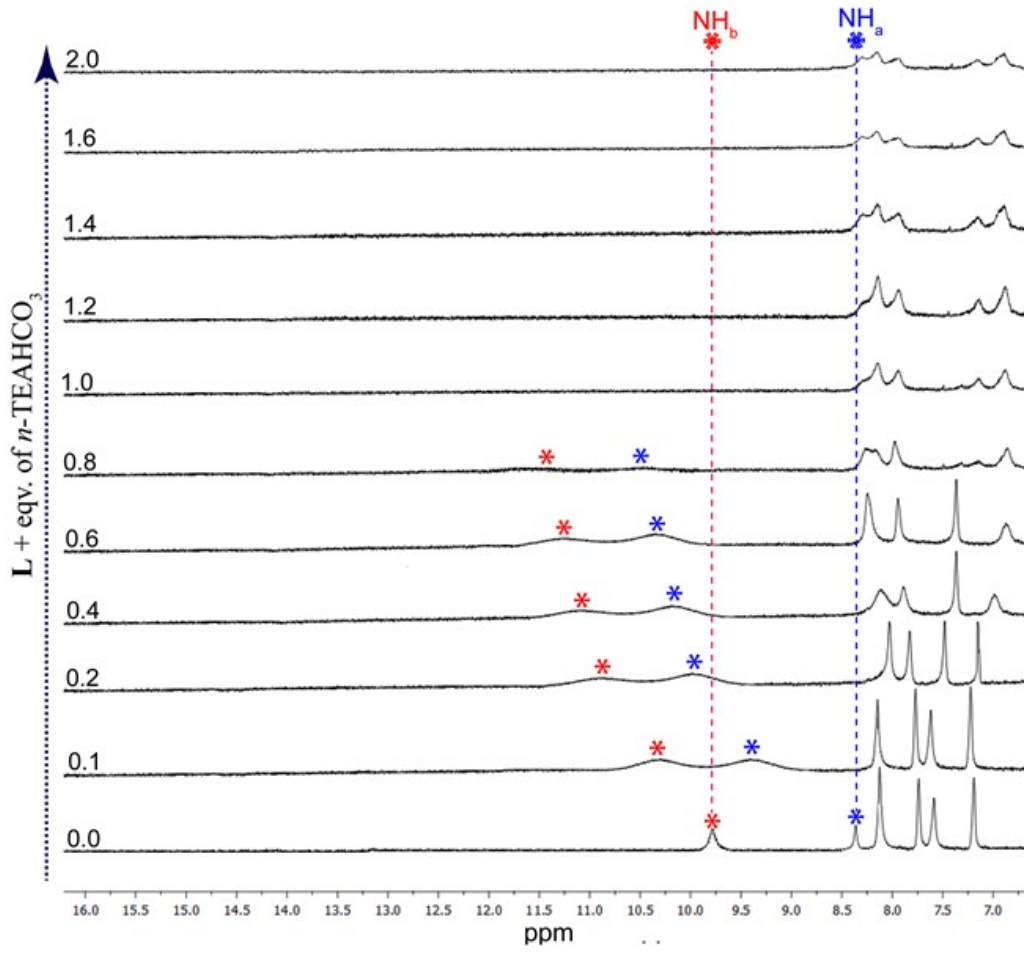

Figure S47. Expanded partial ^{1}H-NMR spectra of **L** upon titration with *n*-$TEAHCO_3$ in DMSO-d_6. Disappearance and broadening of urea –NH peaks due to deprotonation.

Table S1. Hydrogen bonding distances (Å) and Bond angles (°) in the complexes (**1a, 1b, 1c, 2a, 2b** and **2c**):

Complex	D–H···A	*d*(D···H)/ Å	*d*(H···A)/ Å	*d*(D···A)/Å	<D–H···A/°	Symmetry codes
L	N1-H1N···O3	0.86	2.03	2.842(4)	157	1-x,1-y,1-z
	N2-H2N···O3	0.86	2.15	2.947(5)	154	1-x,1-y,1-z
	N3-H3N···O4	0.86	2.31	3.034(4)	143	1+x,y,z
	N4-H4N···O4	0.86	1.95	2.790(5)	164	1+x,y,z
	C25-H25B···O1	0.96	2.57	3.443(7)	152	x,-1+y,z
1	N1-H1N···F13	0.86	1.91	2.760(6)	168	-x,1-y,1-z
	N2-H2N···O3	0.86	2.05	2.900(6)	168	-x,1-y,1-z
	N3-H3N···O3	0.86	2.53	3.290(7)	148	-x,1-y,1-z
	N4-H4NA···F13	0.86	1.85	2.665(8)	156	x,y,z
	N4-H4NB···F13	0.86	1.88	2.665(8)	152	x,y,z
	O3-H3OA···F13	0.85	1.89	2.652(6)	148	x,y,z
	C33-H33B···F11B	0.97	2.52	3.485 (15)	178	x,3/2-y,-1/2+z
	C35-H35A···O2	0.97	2.50	3.428(11)	145	-x,-1/2+y,1/2-z
	C37-H37B···O3	0.97	2.43	3.360(8)	161	x,y,z
2a	N1-H1N···Cl1	0.86	2.63	3.268(3)	132	x,y,z

	N2-H2N···Cl1	0.86	2.40	3.208(3)	157	1-x,1-y,-z
	N3-H3N···Cl1	0.86	2.62	3.432(3)	157	x,y,z
	N4-H4N···Cl1	0.86	2.35	3.201(3)	170	x,y,z
	C25-H25A···O1	0.97	2.53	3.244(5)	130	x,1/2-y,1/2+z
	C29-H29B···O1	0.97	2.48	3.245(5)	136	x,1/2-y, 1/2+z
2b	N1-H1N···Cl1	0.86	2.71	3.304(3)	127	x,y,z
	N2-H2N···Cl1	0.86	2.40	3.251(4)	169	-x,1-y,1-z
	N3-H3N···Cl1	0.86	2.71	3.288(4)	151	x,y,z
	N4-H4N···Cl1	0.86	2.38	3.233(4)	172	x,y,z
3	N1-H1N···Br1	0.86	2.51	3.362(5)	171	x,y,z
	N2-H2N···Br1	0.86	2.77	3.588(5)	158	x,y,z
	N3-H3N···Br1	0.86	2.55	3.326(5)	150	-x,1-y,1-z
	N4-H4N···Br1	0.86	2.76	3.380(5)	131	x,y,z
	C29-H29A···O2	0.97	2.55	3.360(9)	141	x,1/2-y,-1/2+z
	C37-H37A···O2	0.97	2.53	3.339(9)	140	x,1/2-y,-1/2+z
4	N1-H1N···I1	0.86	2.93	3.555(14)	131	x,y,z
	N2-H2N···I1	0.86	2.83	3.517(12)	138	-x,1-y,1-z
	N3-H3N···I1	0.86	3.02	3.830(12)	158	x,y,z
	N4-H4N···I1	0.86	2.76	3.607(13)	170	x,y,z
	C33-H33B···O1	0.97	2.57	3.40 (2)	143	x,3/2-y,-1/2+z
5	N1-H1N···O3	0.86	1.87	2.686(4)	158	x,y,z
	N2-H2N···O4	0.86	2.27	3.051(5)	151	x,y,z
	N3-H3N···O4	0.86	1.87	2.689(5)	159	x,y,z
	N4-H4N···O4	0.86	2.21	2.943(6)	142	x,y,z
	N4-H4N···O4	0.86	2.53	3.357(5)	162	3/2-x,1/2-y,z
	C33-H61A···O1	0.97	2.48	3.387(5)	156	-1+x,y,z
	C35-H63B···O1	0.97	2.56	3.450(5)	152	-1+x,y,z
6	N1-H1N···O6	0.86	2.01	2.84(9)	158	x,y,z
	N2-H2N···O6	0.86	2.18	2.96(8)	151	x,y,z
	N3-H3N···O5	0.86	2.18	2.95(8)	149	x,y,z
	N4-H4N···O5	0.86	2.07	2.87(9)	154	x,y,z
	N5-H5N···O6	0.87	1.99	2.83(10)	162	x,y,z
	N6-H6N···O7	0.86	1.97	2.83(10)	173	x,y,z
	N7-H7N···O7	0.86	2.12	2.94(9)	159	x,y,z
	N8-H8N···O8	0.86	1.91	2.76(9)	169	x,y,z
	C45-H45···F24	0.92	2.52	3.44(14)	174	1-x,-y,1-z
	C58-H58B···O3	0.98	2.55	3.47(12)	158	x,y,z
	C65-H65C···O4	0.97	2.50	3.43(16)	161	x,y,z
	C69-H69A···O5	1.10	2.20	3.22(14)	176	1+x,y,z

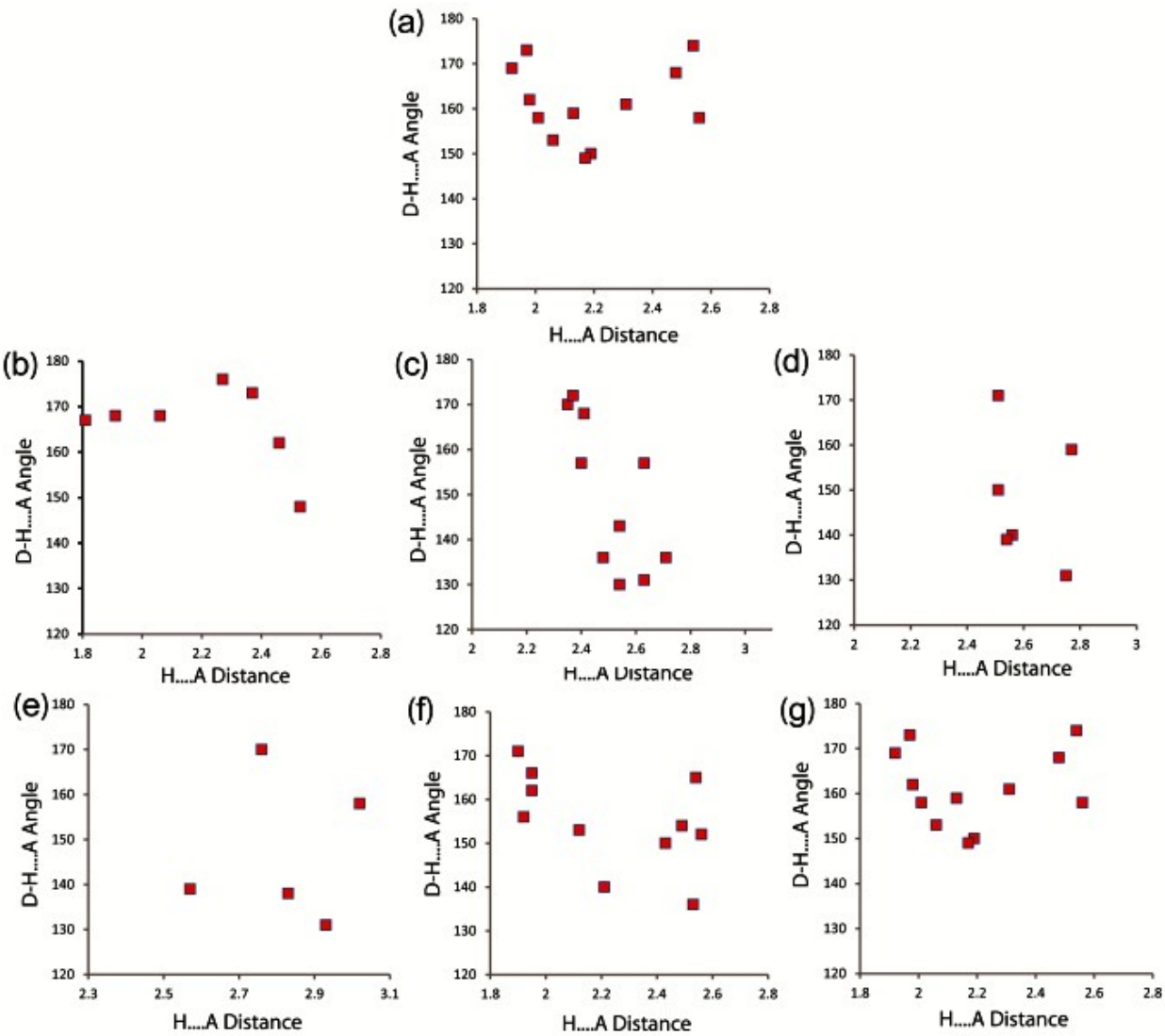

Figure S48. The scatter plot of D−H···A angle vs. H···A distance of the hydrogen bonds in the (a) free receptor **L** (b) complex **1**, (c) complex **2a** and **2b**, (d) complex **3**, (e) complex **4**, (f) complex **5** and (g) complex **6**.

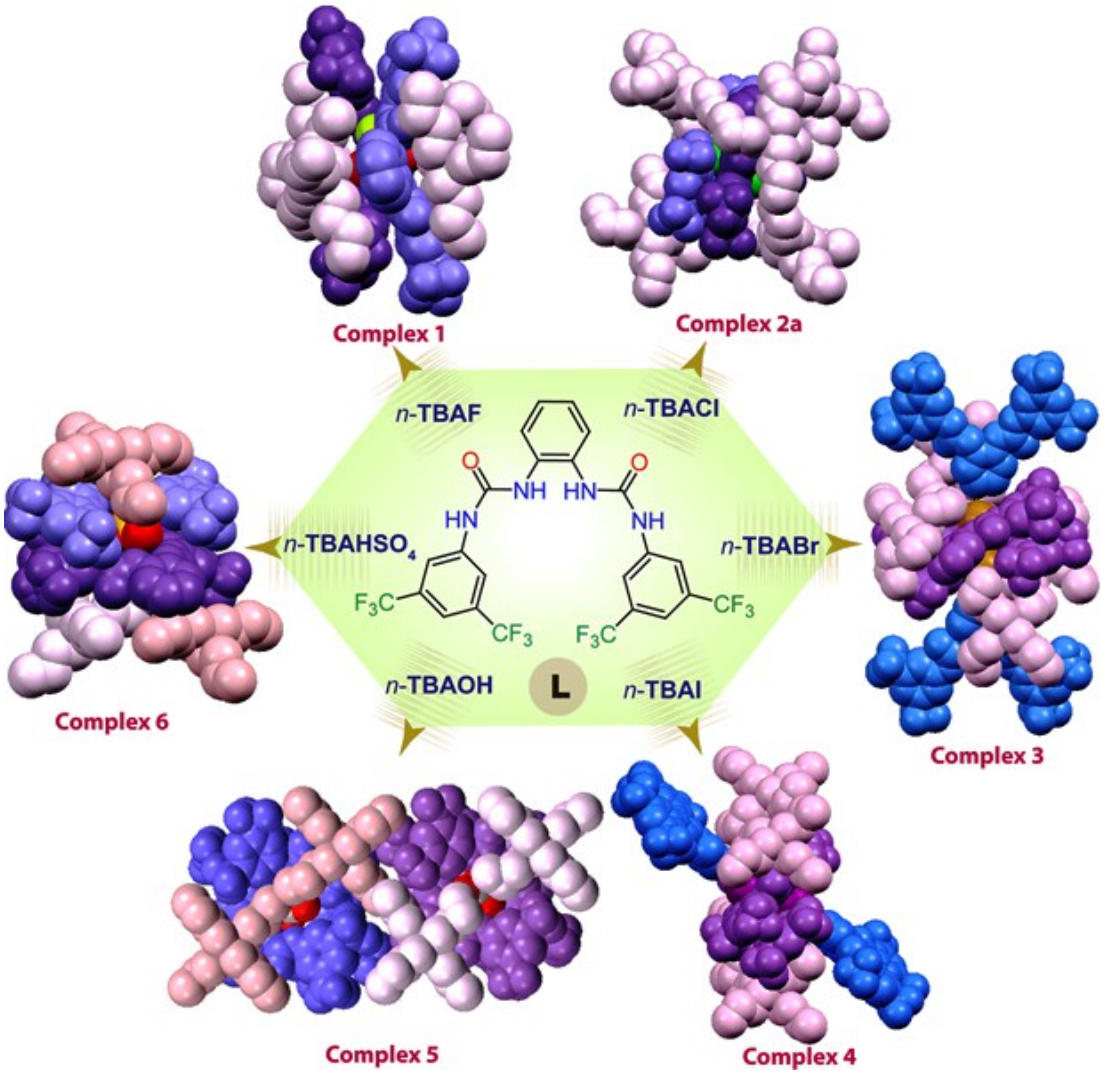

Scheme S49: Partial X-ray structures in space-fill model of all anion complexes depicting systematic and consistent anion binding uniformity of *meta*-disubstituted receptors toward spherical fluoride(hydrated), chloride, bromide, iodide, planar carbonate and tetrahedral sulphate anions.

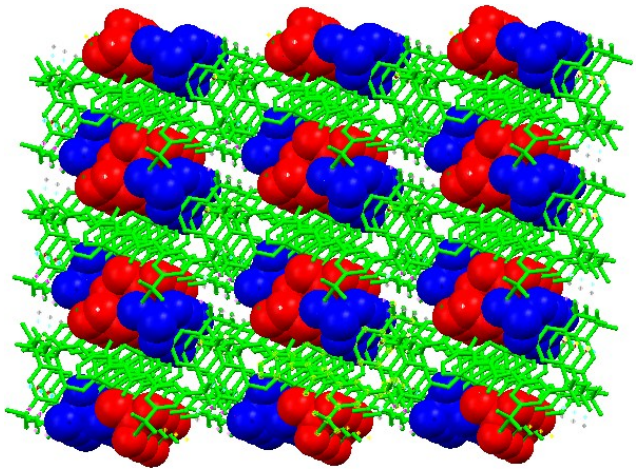

Figure S50. X-ray structures of DMSO solvated free receptor **L** depicting packing motif as viewed down from crystallographic *b* axis by symmetry equivalence.

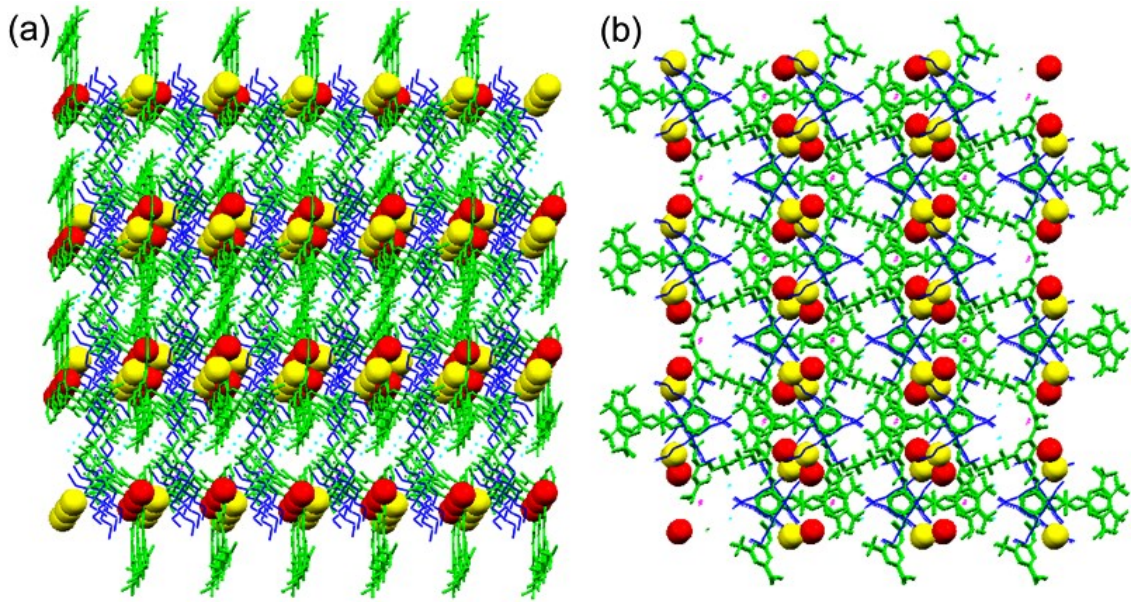

Figure S51. X-ray structures depicting (a) packing motif of hydrated receptor-fluoride (*n*-TBA countercation) complex **1** as viewed down from crystallographic *b* axis by symmetry equivalence and (b) packing motif along the crystallographic *c* axis by symmetry equivalence.

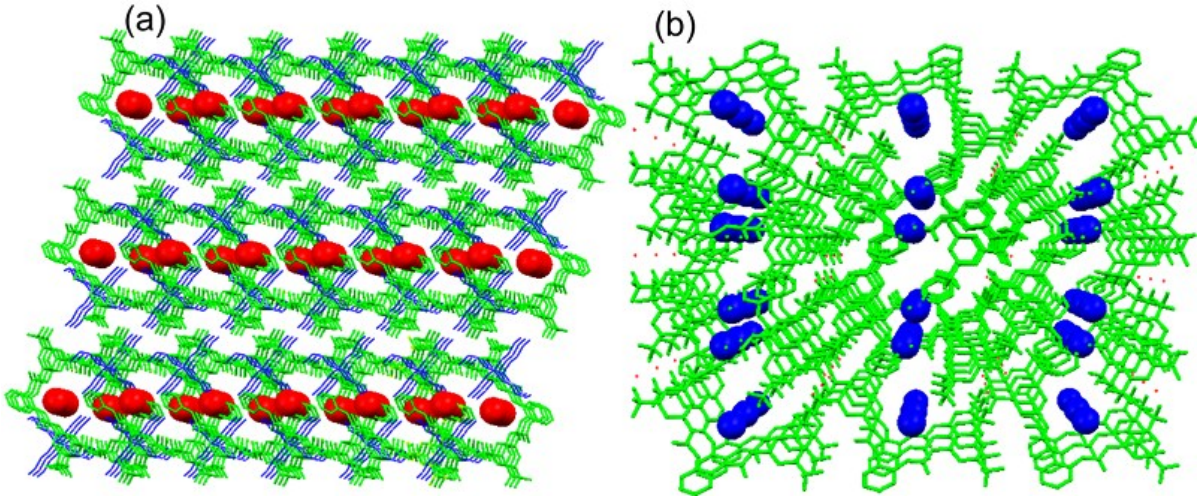

Figure S52. X-ray structures depicting (a) packing motif of 2:2 **L**-Chloride (*n*-TBA countercation) complex **2a** as viewed down from crystallographic *b* axis by symmetry equivalence and (b) packing motif of 2:2 **L**-Cl (TEA countercation) complex **2b** as viewed down from crystallographic *b* axis by symmetry equivalence.

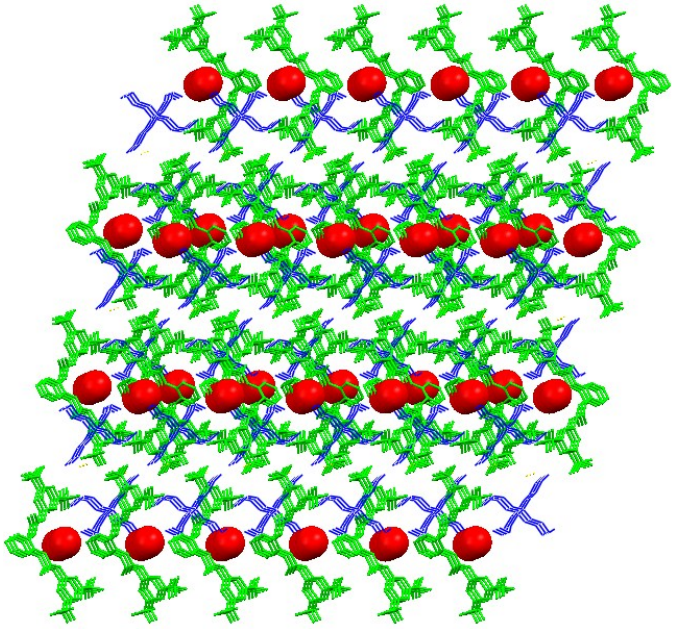

Figure S53. X-ray structures depicting packing motif of 2:2 **L**-bromide (*n*-TBA countercation) complex **3** as viewed down from crystallographic *b* axis by symmetry equivalence.

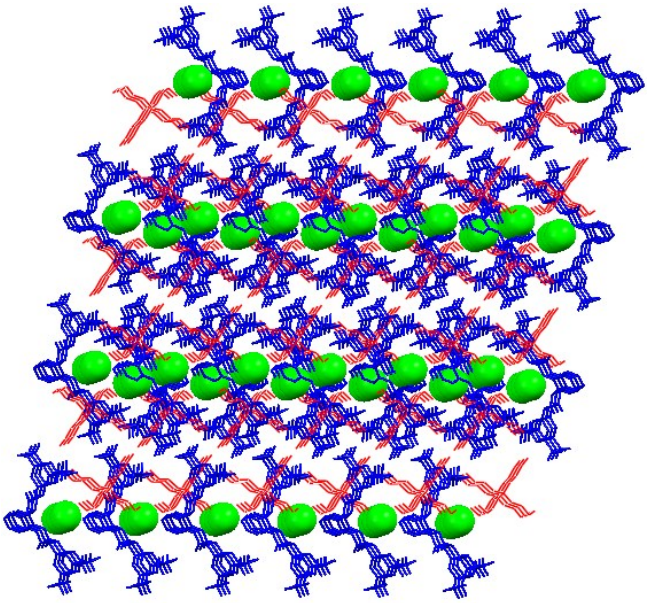

Figure S54. X-ray structures depicting packing motif of 2:2 **L**-iodide (*n*-TBA countercation) complex **4** as viewed down from crystallographic *b* axis by symmetry equivalence.

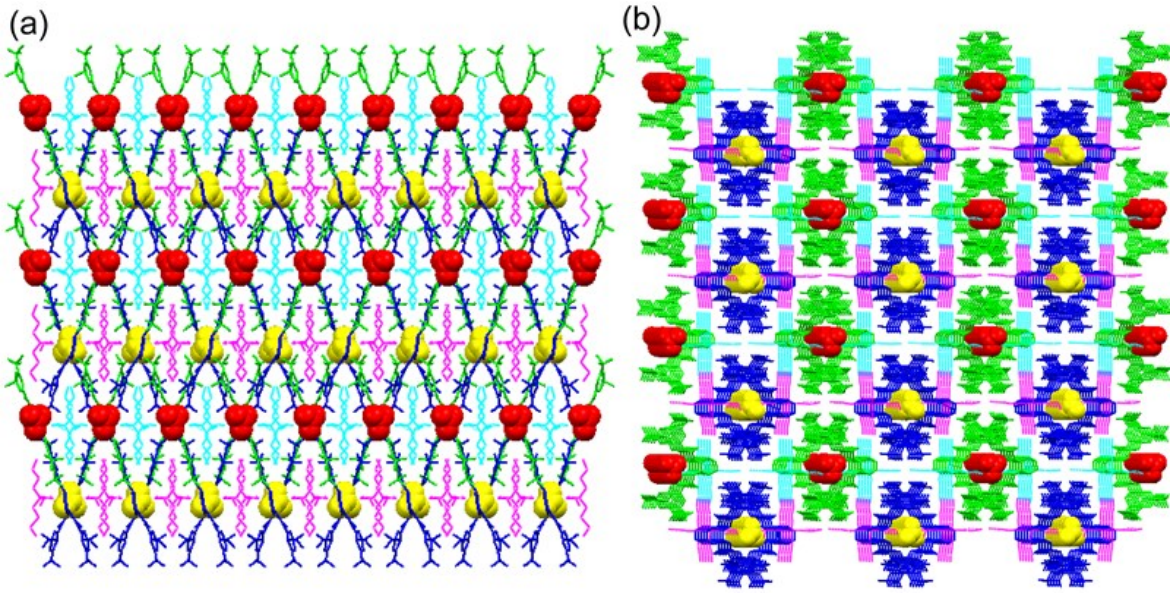

Figure S55. X-ray structures depicting packing motif of 2:1 **L**-carbonate (*n*-TBA countercation) complex **5** as viewed down from crystallographic *b* axis.

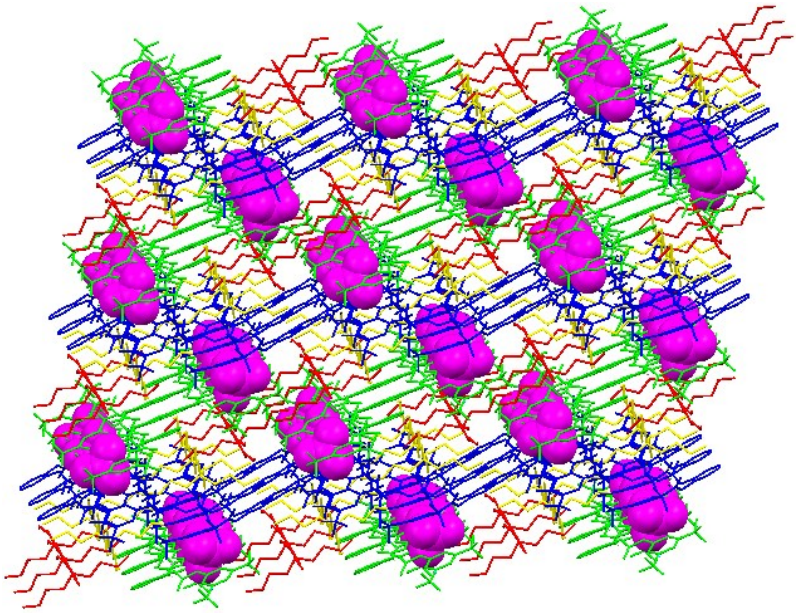

Figure S56. X-ray structures depicting packing motif of 2:1 **L**-sulphate (*n*-TBA countercation) complex **6** as viewed down from crystallographic *b* axis by symmetry equivalence.